High-throughput assessment identifying major platelet Ca2+ entry pathways via tyrosine kinase-linked and G protein-coupled receptors

Please check the document version of this publication:

• A submitted manuscript is the version of the article upon submission and before peer-review. There can be important differences between the submitted version and the official published version of record. People interested in the research are advised to contact the author for the final version of the publication, or visit the DOI to the publisher's website.
• The final author version and the galley proof are versions of the publication after peer review.
• The final published version features the final layout of the paper including the volume, issue and page numbers.

Link to publication

Download date: 27 Apr. 2024

High-throughput assessment identifying major platelet Ca²⁺ entry pathways via tyrosine kinase-linked and G protein-coupled receptors

Hilaire Yam Fung Cheung [a,b,c,1], Jinmi Zou [a,d,1], Chukiat Tantiwong [a,e], Delia I. Fernandez [a,f], Jingnan Huang [a,b,f], Robert Ahrends [b,g], Mark Roest [d], Rachel Cavill [h], Jon Gibbins [e], Johan W. M. Heemskerk [a,d,*]

[a] Department of Biochemistry, Cardiovascular Research Institute Maastricht (CARIM), Maastricht University, Maastricht, The Netherlands
[b] Leibniz-Institut für Analytische Wissenschaften-ISAS-e.V, Dortmund, Germany
[c] Institute of Cardiovascular Sciences, College of Medical and Dental Sciences, University of Birmingham, Birmingham, United Kingdom
[d] Synapse Research Institute Maastricht, 6217 KD Maastricht, The Netherlands
[e] Institute for Cardiovascular and Metabolic Research (ICMR), School of Biological Sciences, University of Reading, Reading, United Kingdom
[f] Center for Research in Molecular Medicine and Chronic Diseases (CIMUS), Universidade de Santiago de Compostela, Santiago de Compostela, 15706, Spain
[g] Dept. of Analytical Chemistry, University of Vienna, Vienna, Austria
[h] Department of Advanced Computing Sciences, Maastricht University, 6229 ER Maastricht, The Netherlands

ARTICLE INFO

ABSTRACT

In platelets, elevated cytosolic Ca²⁺ is a crucial second messenger, involved in most functional responses, including shape change, secretion, aggregation and procoagulant activity. The platelet Ca²⁺ response consists of Ca²⁺ mobilization from endoplasmic reticulum stores, complemented with store-operated or receptor-operated Ca²⁺ entry pathways. Several channels can contribute to the Ca²⁺ entry, but their relative contribution is unclear upon stimulation of ITAM-linked receptors such as glycoprotein VI (GPVI) and G-protein coupled receptors such as the protease-activated receptors (PAR) for thrombin. We employed a 96-well plate high-throughput assay with Fura-2-loaded human platelets to perform parallel $[Ca^{2+}]_i$ measurements in the presence of EGTA or CaCl₂. Per agonist condition, this resulted in sets of EGTA, CaCl₂ and Ca²⁺ entry ratio curves, defined by six parameters, reflecting different Ca²⁺ ion fluxes. We report that threshold stimulation of GPVI or PAR, with a variable contribution of secondary mediators, induces a maximal Ca²⁺ entry ratio of 3–7. Strikingly, in combination with Ca²⁺-ATPase inhibition by thapsigargin, the maximal Ca²⁺ entry ratio increased to 400 (GPVI) or 40 (PAR), pointing to a strong receptor-dependent enhancement of store-operated Ca²⁺ entry. By pharmacological blockage of specific Ca²⁺ channels in platelets, we found that, regardless of GPVI or PAR stimulation, the Ca²⁺ entry ratio was strongest affected by inhibition of ORAI1 (2-APB, Synta66) > Na⁺/Ca²⁺ exchange (NCE) > P2×₁ (only initial). In contrast, inhibition of TRPC6, Piezo1/2 or STIM1 was without effect. Together, these data reveal ORAI1 and NCE as dominating Ca²⁺ carriers regulating GPVI- and PAR-induced Ca²⁺ entry in human platelets.

1. Introduction

Increased cytosolic Ca²⁺ is a crucial second messenger, involved in essentially all functional platelet responses, ranging from shape change, spreading, adhesion by integrin activation, dense and alpha-granule secretion, platelet aggregation and thrombus assembly up to the processes of clot retraction and development of platelet procoagulant activity [1–4]. Most platelet agonists induce a rise in cytosolic $[Ca^{2+}]_i$ to steer a variety of signaling pathways, in order to regulate actin and

tubulin cytoskeleton reorganization, small molecular weight GTPase activation, networks of protein kinases and phosphatases, calpain protease activation, secretome organization, thromboxane release, and phospho-inositide and other phospholipid alterations [5–8].

In situations of hemostasis and thrombosis, platelet Ca²⁺ signaling can be evoked by ITAM-linked receptors (ILR) acting through protein tyrosine kinases, as well as by G-protein coupled receptors (GPCR) working the Gqα and Giα proteins [9]. Regarding ILR, the collagen receptor glycoprotein VI (GPVI) has been extensively studied in the

context of thrombosis and hemostasis, with several anti-GPVI drugs being evaluated in clinical trials [10]. Vascular collagens and the soluble mimetic collagen-related peptide (CRP), as established GPVI agonists, operate via tyrosine phosphorylation and activation of phospholipase Cγ2 (PLCγ2) [11]. On the other hand, activation of platelet GPCR in particular occurs by soluble agonists, like thrombin (acting via PAR1 and PAR4), ADP (acting via $P2Y_1$ and $P2Y_{12}$) and thromboxane A_2 (acting via TP receptors). The common activation mechanism is Gqα-mediated activation of PLCβ isoforms with an additional Giα-mediated activation phosphoinositide 3-kinases [2,4,12]. Drugs interfering with these GPCR pathways are regularly prescribed to patients with prior cardiovascular disease. The success of the so-called secondary mediator inhibitors (SMI) - i.e. aspirin to block thromboxane synthesis and ADP-receptor antagonists - relies on the fact that they suppress amplification mechanisms, rather than primary processes of platelet activation [10,13].

In human and mouse platelets, classical Ca^{2+}-signaling mechanisms operate, i.e. primary internal Ca^{2+} mobilization and secondary store-operated Ca^{2+} entry (SOCE) or receptor-operated Ca^{2+} entry (ROCE), such as reviewed recently [4]. These pathways are crucially involved in platelet-dependent immune responses, intravascular thrombosis formation and thrombo-inflammation in mouse, and by extension also in man [4,14,15]. In brief, PLCβ/γ activity results in the formation of inositol 1,4,5 trisphosphate ($InsP_3$), which by way of a Ca^{2+}-induced Ca^{2+} release stimulates the $InsP_3$-operated Ca^{2+} channels in the endoplasmic reticulum. Pumping back of the released Ca^{2+} from the cytosol into Ca^{2+} stores occurs by sarco- and endoplasmic reticulum Ca^{2+}-ATPases (SERCAs), which are selectively inhibited by thapsigargin, a compound that prolonges the $[Ca^{2+}]_i$ signal [9,16].

Regarding SOCE, a important role in platelets has been confirmed for the Ca^{2+} channel ORAI1 [17], which via the BIN2 protein couples to the Ca^{2+} store sensor STIM1 [18]. This mechanism contributes to both the ILR- and GPCR-induced Ca^{2+} entry [4,19,20]. It has been shown that platelets from mice with a defect in STIM1, BIN2 or ORAI1 display impaired Ca^{2+} responses with common agonists [20–23]. The low platelet Ca^{2+} responses were accompanied by a protection against arterial thrombus formation in vivo and a lowered collagen-dependent thrombus formation in vitro [4]. Similarly, in blood from immunodeficient patients with a loss-of-function mutation in *ORAI1* or *STIM1,* in vitro thrombus formation on collagen was found to be impaired [24]. Yet, other studies suggest the operation of additional ROCE pathways in platelets as well [23,25].

Established for platelet activation is also the $P2\times_1$ cation channel, as a fast way to increase $[Ca^{2+}]_i$, in response to the secondary mediator ATP [26,27]. Other papers indicate that a significant proportion of the diacylglycerol-induced ROCE in platelets is carried by transient receptor potential C (TRPC) type of cation channels, TRPC3 and TRPC6, so far with an unclear contribution to hemostasis and thrombosis [28,29]. The murine TRPC6 protein appeared to support the ORAI1-dependent SOCE mechanism [30]. Additional proteins with a possible contribution to Ca^{2+} entry in platelets are the mechanosensitive Piezo1/2 ion channels [31], and Na^+/Ca^{2+} exchangers (NCE) operating in reverse mode [32].

While several channel types are considered to contribute to SOCE and ROCE in human platelets, their relative strength and contribution to the agonist-induced Ca^{2+} entry process are unknown. In the present paper, we investigated this in Fura-2-loaded platelets by parallel measurements of $[Ca^{2+}]_i$ in the presence of external EGTA or $CaCl_2$, thus blocking or allowing Ca^{2+} entry, respectively, using a previously established 96-well plate-based high throughput assay [33]. For the studies we used two GPVI (ILR) agonists, i.e. CRP and collagen, and two PAR (GPCR) agonists, thrombin and TRAP, as well as the SERCA inhibitor thapsigargin. By systematic comparison of the Ca^{2+} entry traces we were able to directly compare the effects of pharmacological blockage of ORAI1, STIM1, TRPC6, $P2X_1$, Piezo1/2 or NCE.

2. Materials and methods

2.1. Materials

Thrombin was obtained from Enzyme Research Laboratories (South Bend IN, USA). Thrombin receptor-activating peptide SFLLRN (TRAP) was purchased from Bachem (Bubendorf, Switzerland); cross-linked collagen-related peptide (CRP) came from the University of Cambridge (Cambridge, United Kingdom); Fura-2 acetoxymethyl ester and human fibrinogen were obtained from Invitrogen (Carlsbad, CA, USA); Pluronic F-127 from Molecular Probes (Eugene OR, USA). 2-aminoethyl diphenylborinate (2-APB) and ORM-10,103, 2-[(3,4-*dihydro*-2-*phenyl*-2H-1-*benzopyran*-6-*yl*)*oxy*]−5-nitro-pyridine were from Sigma-Aldrich (St. Louis, MO, USA), GsMTx4 was from Tocris Bioscience (Bristol, United Kingdom), MRS-2159 from Santa-Cruz (Santa-Cruz, CA, USA), ML-9 and BI-749,327 were from MedChem Express (Monmouth Junction, NJ, USA). Human α-thrombin came from Kordia (Leiden, The Netherlands). Standard Horm-type collagen (dissolved in 0.1 M acetic acid) was obtained from Nycomed (Hoofddorp, The Netherlands). Synta-66, 3-fluoropyridine-4-carboxylic acid (2′,5′-dimethoxybiphenyl-4-yl)amide, came from GlaxoSmithKline (London, UK). The PAR4-activating peptide AYPGKF-NH$_2$ was a kind gift of Synpeptide Ltd. (Pudong, Shanghai, China). Other materials were from sources, described before [34].

2.2. Subjects and blood collection

Blood was taken by venipuncture from healthy male and female volunteers who had not taken anti-platelets in the previous ten days, after full informed consent according to the Helsinki declaration. The study was approved by the Medical Ethics Committee of Maastricht University. According to the approval, blood donor age and sex were not recorded. Blood was collected into 3.2% sodium citrate (Vacuette tubes, Greiner Bio-One, Alphen a/d Rijn, the Netherlands). Blood donors had platelet counts within the reference range, as measured with a Sysmex XN-9000 analyzer (Sysmex, Kobe, Japan).

2.3. Platelet isolation and loading with Fura-2

Platelet-rich plasma (PRP) and washed platelets were obtained from citrated blood, as described earlier [23,35]. PRP was obtained through centrifugation of blood samples at 260 g for 10 min, after supplementation of 1:10 vol/vol acid citrate dextrose (ACD; 80 mM trisodium citrate, 183 mM glucose, 52 mM citric acid). The collected PRP was then centrifuged in eppendorf tubes at 2360 g for 2 min. The pelleted platelets were resuspended into HEPES buffer pH 6.6 (10 mM HEPES, 136 mM NaCl, 2.7 mM KCl, 2 mM $MgCl_2$, 5.5 mM glucose, and 0.1% bovine serum albumin). After addition of apyrase (1 U/mL) and 1:15 vol/vol ACD to the platelet suspension, another centrifugation step was performed to obtain washed platelets. Based on an earlier protocol [36], the washed platelets resuspended into HEPES buffer pH 7.45 at a count of 2 × 10^8/mL were loaded with Fura-2 acetoxymethyl ester (3 μM) and pluronic F-127 (0.4 μg/mL) for 40 min at room temperature. In comparison to a previous protocol, the loading at room temperature and the pre-mixing of probe with Pluronic F-127 prevented accumulation of de-esterified dye in the intracellular organelles [37]. Once loaded with Fura-2, the cells were centrifuged in the presence of apyrase (1 U/mL) and 1:15 vol/vol ACD. The final platelet count after resuspension into HEPES buffer pH 7.45 was 2 × 10^8/mL. Adequacy of Fura-2 loading in the cytoplasm was confirmed by *a* >90% quenching of the isosbestic Fura-2 signal (360 nm excitation) with $MnCl_2$ [16]. In addition, microscopic examination of spread platelets did not show compartmentalization of the Fura-2 fluorescence.

The commonly used procedure of ACD and apyrase silencing of platelets prevented autocrine activation, while maintaining resting cyclic-AMP levels [38]. Platelet activation markers (P-selectin and PAC1 antigen) were <2% using the platelet isolation procedure [39].

2.4. Calibrated high-throughput platelet [Ca^{2+}]$_i$ measurements

Changes in [Ca^{2+}]$_i$ of Fura-2-loaded platelets were measured in 96-well plates using a FlexStation 3 robot (Molecular Devices, San Jose, CA, USA), basically as described [33,40]. The Xenon flash light-based measurements of fluorescence, in combination with the excellent optics of the FlexStation3 reader chip allowed to measure with limited fluorescence bleaching.

In brief, 200 μL samples of platelets (2 × 10^8/mL) per well were left untreated or were pretreated with apyrase (0.1 U/mL) and indomethacin (20 μM) for 10 min at room temperature. Where indicated, pharmacological inhibitors to block Ca^{2+} entry were added (at room temperature) (see Table 1). After the addition of either 0.1 mM EGTA or 2 mM CaCl$_2$, the platelets in wells were temperature adjusted (37 °C), and fluorescence was recorded at two excitation wavelengths for 10 min. During the measurements, 20 μL of agonist solution was added by automated pipetting. Note that the mixing of agonist with Fura-2-loaded platelets was diffusion-limited, and occurred by high-speed injection of 10% volume of the agonist solution. Prior to default use, injection volume and speed (125 μL/s) was optimized as to obtain maximal platelet responses [33].

Changes in Fura-2 fluorescence (37 °C) were measured per row by ratiometric fluorometry, using excitation wavelengths of 340 and 380 nm and a single emission wavelength of 510 nm [33]. Fura-2 fluorescence ratio values per well were obtained every 4 s. Separate calibration wells contained Fura-2-loaded platelets that were lysed with 0.1% Triton-X-100 in the presence of either 1 mM CaCl$_2$ or 1 mM EGTA/Tris for determining R$_{max}$ and R$_{min}$ values [35]. After the correction for 340 and 380 nm background fluorescence levels, nanomolar changes in [Ca^{2+}]$_i$ were calculated according to the Grynkiewicz equation with a K$_d$ of 224 nM [41]. All measurements were completed within 2–3 h of isolation of cells.

For the present measurements, the loading concentration with Fura-2 AM was optimized, giving a stable calibrated Ca^{2+} responses at 1.5 to 3 μM, and highest 340 nm fluorescent agonist signals (+22%, $n = 3$) and lowest a noise at 3 μM. Dye leakage from the platelets appeared to be negligible; this was observed by a minimal, <5 nM apparent [Ca^{2+}]$_i$ rise upon addition of 1 mM CaCl$_2$ to unstimulated cells.

For the relative assessment of Ca^{2+} entry, activation experiments were routinely performed in parallel (duplicate) wells, containing either 0.1 mM EGTA or 2 mM CaCl$_2$. Accordingly, after calibration, sets of nM

Table 1
Platelet agonists, receptors and channels reported to modulate Ca^{2+} responses. For full inhibitor names, see methods section. Protein copy numbers per platelet were taken from Ref. [68].

Compound	1st target	Copies	2nd targets	Ref. conc.	Ref.
Agonists					
CRP	GPVI	9577	n.a.	0.1–30 μg/mL	[33]
Collagen	GPVI	9577	α2β1	1–10 μg/mL	[40]
Thrombin	PAR1/4	n.a./1095	GPIbα	0.3–30 nM	[33]
TRAP	PAR1	n.a.	n.a.	0.5–15 μM	[33]
Modulators					
SMI*	P2Y$_1$, COX1	~1000	P2Y$_{12}$	0.1 U/mL,20μM	[33]
Thapsigargin	SERCA2b	25,272	SERCA3	1 μM	[24]
Channel inhibitors					
2-APB	ORAI1	1658	InsP$_3$ R**	10 μM	[49]
BI-749,327	TRPC6	1101	n.a.	0.1 μM	[52]
GsMTx4	Piezo1/2	2***	n.a.	3 μM	[31]
ML-9	STIM1	7423	MLCK, Akt	30 μM	[50]
MRS-2159	P2X$_1$	1441	P2Y$_1$	1 μM	[27]
ORM-10,103	NCX3	578	NCX1	10 μM	[32]
Synta66	ORAI1	1658	n.a.	10 μM	[49]

*SMI, secondary mediator inhibitors (indomethacin + apyrase); **InsP$_3$ receptor types 1–3 (4873 copies); ***for mouse platelets [69]; n.a., not available.

[Ca^{2+}]$_i$ traces were obtained without (EGTA) or with (CaCl$_2$) Ca^{2+} entry.

2.5. Data analysis and molecular calculations

The nanomolar [Ca^{2+}]$_i$ traces (4–6 s intervals during 600 s) were floating-point averaged before further processing. Per agonist and inhibitor condition, then ratioed Ca^{2+} entry traces were calculated. These were obtained by dividing the nanomolar traces in the presence of CaCl$_2$ by the corresponding traces in the presence of EGTA. Taking into account the assumptions mentioned below, the ratioed [Ca^{2+}]$_i$ traces represent the relative amount of Ca^{2+} entry per unit of intracellular Ca^{2+} release (Eq. 1):

$$\frac{[Ca]i \text{ in } CaCl2}{[Ca]i \text{ in } EGTA} = \frac{ER \text{ release} + Entry}{ER \text{ release}} = 1 + \frac{Entry}{ER \text{ release}}$$

Using a script in Excel, the [Ca^{2+}]$_i$ traces with CaCl$_2$ or EGTA were analyzed on six curve parameters: the nM levels at start (P1), at first peak (P4) and final (P6); the initial slope after agonist addition as nM/s (P2) and the change of slope (P3); furthermore, the agonist-induced increase in area-under-curve over 600 s (P5). For the Ca^{2+} entry ratio curves, these curve parameters were calculated as well.

The following assumptions were used for the molecular calculation of Ca^{2+} fluxes in a representative platelet (of average size). Mean platelet volume (average from 96 volunteers) was set at 10.24 fL [42]. Based on electron microscopic images [43], the volume contribution of intracellular organelles and open canicular system was set at 20%, which resulted in a mean cytosolic volume of 8.92 fL. For 0.4 × 10^8 platelets per well, this gave a total cytosolic volume of 3.57 × 10^{-7} L. Considering the single-platelet cytosolic volume of 8.92 fL, then a [Ca^{2+}]$_i$ increase of 1 nM represents 8.92 × 10^{-24} mol, i.e. 5.37 mobilized Ca^{2+} ions per single platelet.

Considerations for interpretation of the [Ca^{2+}]$_i$ traces were as follows. *(i)* In Fura-2-loaded platelets, the low resting [Ca^{2+}]$_i$ was set at ~20 nM. *(ii)* Rises in [Ca^{2+}]$_i$ in response to agonists were considered to be the mathematical summation of InsP$_3$-induced Ca^{2+} release from the endoplasmic reticulum (ER, taken as one undivided compartment) and from extracellular Ca^{2+} entry via ion channels and exchangers. This implies that any enforcement of InsP$_3$ channel activity by extracellular CaCl$_2$ via Ca^{2+}-induced Ca^{2+} release [1] is attributed to the entry part. Concerning the mitochondrial and lysosomal Ca^{2+} compartments, of which the sizes and regulation are poorly established [4], these are considered as a providing a fixed fractional contribution to the total Ca^{2+} stores, not contributing to InsP$_3$-induced Ca^{2+} release. *(iii)* It is thus assumed that measurements in the presence of 0.1 mM EGTA reflect only intracellular Ca^{2+} release, while measurements in the presence of 2 mM CaCl$_2$ reflect the summed contribution of intracellular Ca^{2+} release and extracellular Ca^{2+} entry. *(iv)* By using suspensions of 0.4 × 10^8 platelets, intercellular heterogeneity due to single-cell oscillations will be averaged out [44]. *(v)* Transient decreases in [Ca^{2+}]$_i$ are considered to result from the combined Ca^{2+}-ATPase activities of SERCA and PMCA (plasma membrane Ca^{2+}-ATPases) isoforms, unless indicated otherwise. *(vi)* In calculations, the cytosolic Ca^{2+}-buffering capacity of Fura-2 and the likely fractional uptake into mitochondria were discarded. *(vii)* Finally, the maximal [Ca^{2+}]$_i$ level to be achieved was set at 200 × K$_d$ (44.8 μM).

2.6. Pharmacologic inhibition of Ca^{2+} responses

An overview of relevant platelet receptors and channels with protein copy numbers is provided in Table 1. The table also contains the compounds reported to block Ca^{2+} channels or exchangers with reasonable selectivity at indicated concentration. In experiments with Fura-2-loaded platelets in the presence of EGTA or CaCl$_2$, the indicated compounds were always tested versus relevant vehicle solution (final DMSO concentration <0.5%).

2.7. Heatmaps and statistics

Data are expressed as means ± SD. The program GraphPad Prism 8 (San Diego, CA, USA) was used for statistical analyses. Regression analysis was performed with the program R, which was also used for heatmap generation. For heatmap representation, values per curve parameter sets (P1+4 + 6, P2+3, or P5) were univariate-scaled at 0–100% per indicated set of conditions, as indicated in the figure legends. Statistical significance, calculated by a two-tailed *t*-test, was defined as $P < 0.05$.

3. Results

3.1. High Ca^{2+} entry ratio in GPVI-stimulated platelets

To quantify how GPVI-induced extracellular Ca^{2+} entry (via ILR) relied on intracellular Ca^{2+} mobilization in platelets, we performed dose-response experiments, using the strong agonist CRP and the weaker agonist collagen type-I for this receptor [9]. Employing the 96-well plate method with automated agonist injection [33,40], each agonist was added to Fura-2-loaded platelets in the presence of external $CaCl_2$ or

Figure 1
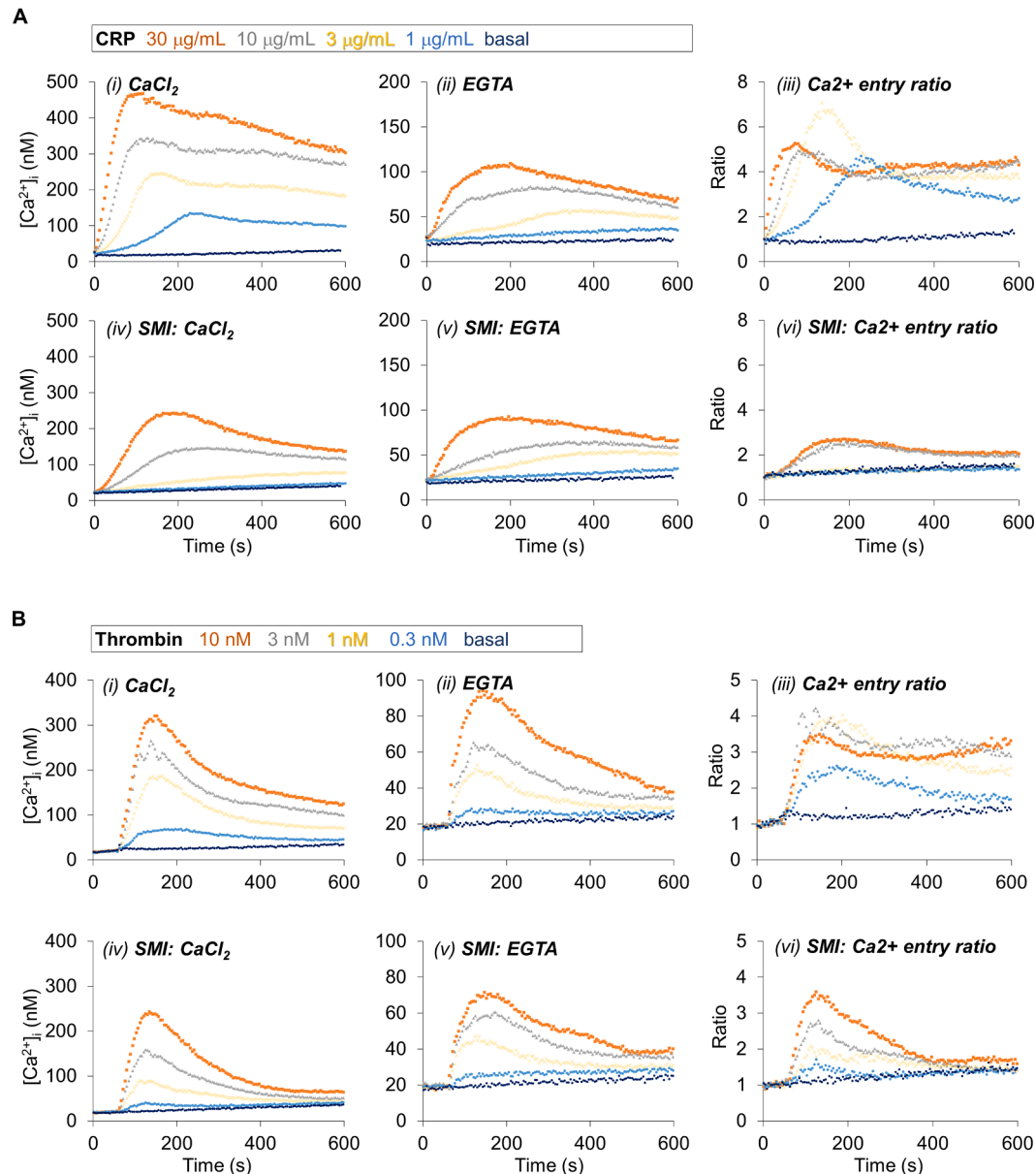
Fig. 1. Dose-dependency of Ca^{2+} entry with strong collagen or thrombin receptor **agonists.** Fura-2-loaded platelets in 96-well plates were left untreated or were pre-incubated with SMI (0.1 U/mL apyrase and 20 μM indomethacin) at room temperature. Roboted stimulation in the presence of 2 mM $CaCl_2$ or 0.1 mM EGTA was with CRP (1–30 μg/mL) or thrombin (0.3–10 nM). Measurements by ratio fluorometry were performed for 600 s using a FlexStation 3, and values were converted into calibrated nM levels of $[Ca^{2+}]_i$. Agonists were injected into wells at 60 s ($t = 0$) and reached platelets in a diffusion-limited way. (**A-B**) Calibrated $[Ca^{2+}]_i$ traces (non-smoothed) upon stimulation with CRP (**A**) or thrombin (**B**), obtained in the absence (**i-iii**) or presence (**iv-vi**) of SMI (non-smoothed). Parallel traces were measured in the presence of $CaCl_2$ (left panels) or EGTA (middle panels). Curves of Ca^{2+} entry ratio (right panels) were obtained by dividing corresponding $CaCl_2$/EGTA curves, representing the relative amount of Ca^{2+} entry over time. Data are representative of at least three experiments ($n = 3$–5 donors). For parameter values, see Suppl. Datafile 1.

EGTA. After calibration we obtained parallel curves of nanomolar rises in $[Ca^{2+}]_i$ for 600 s, either with or without Ca^{2+} entry, which were analyzed for 6 curve parameters (P1, basal nM level; P2, slope to initial peak; P3, change of slope; P4, first nM peak level; P5, area-under-the-activation curve; and P6, final nM level). By ratioing the two parallel curves, we obtained corresponding Ca^{2+} entry ratio curves, which were analzyed for the same parameters.

Platelet stimulation with CRP (1–30 µg/mL) resulted in a dose-dependent increased $[Ca^{2+}]_i$ peak level, followed by a sustained phase in the presence of eiher $CaCl_2$ or EGTA (Fig. 1A i-ii). Quantification versus the reference condition of $CaCl_2$/CRP 10 µg/mL indicated that the first peak level (P4) at all agonist doses was 3–5 fold higher with $CaCl_2$ than with EGTA presence (Table 2). Further comparison of the curves indicated a longer time-to-peak, when the Ca^{2+} entry was eliminated (Fig. 1A i-ii). The Ca^{2+} entry ratio curves showed a dose-dependent enhancement of slope, reaching a maximal level of 4–7 (Fig. 1A iii).

To examine the contribution of autocrine platelet agonists (i.e. released thromboxane A_2 and ADP) to the CRP-induced Ca^{2+} responses, the Fura-2-loaded platelets in wells were pre-incubated with secondary mediator inhibitors (SMI) apyrase (0.1 U/mL) and indomethacin (20 µM), *i.e.* a treatment sufficient to block the autocrine Ca^{2+} release events [45]. At all CRP concentrations, we observed a lowering and delay of the $[Ca^{2+}]_i$ traces, although the SMI effects were relatively larger in the presence of $CaCl_2$ than with EGTA (Fig. 1A iv-v). Quantitation of the first peak indicated a 20–55% reduction with SMI, which percentage increased with the CRP dose in the presence of $CaCl_2$. In contrast, there was a consistent ~25% reduction by SMI in the presence of EGTA (Table 1). Concerning in the Ca^{2+} entry ratio traces, the presence of SMI reduced the curve maximum from 7 to 3 in cases of $\geq$10 µg/mL CRP, while no agonist signal was observed at the lower doses (Fig. 1A vi).

Platelet stimulation with collagen (1–30 µg/mL) in the presence of $CaCl_2$ led to relatively low $[Ca^{2+}]_i$ peak levels (Suppl. Fig. 1A i), not exceeding 9 ± 1% to 19 ± 1% of the peak levels obtained at 10 µg/mL CRP (Table 2). This is in agreement with earlier findings that collagen in platelet suspensions acts as a weak GPVI agonist [40]. The observed flat $[Ca^{2+}]_i$ traces with EGTA indicated that the collagen-induced Ca^{2+} signal relied on Ca^{2+} entry, but with Ca^{2+} ratio curves not exceeding a peak value of 2 (Suppl. Fig. 1A ii-iii). The presence of SMI annulled the collagen-induced $[Ca^{2+}]_i$ traces, indicating a necessarily enforcement by autocrine agonists (Supp. Fig. 1A iv-vi). Jointly, these findings indicated that a certain activation level of GPVI, supported by secondary mediators, needs to be reached to induce a Ca^{2+} entry ratio peak value of 3–7.

3.2. Moderate Ca^{2+} entry ratio in PAR-stimulated platelets

For comparison to the GPVI-induced $[Ca^{2+}]_i$ traces in platelets, we

Table 2
Relative agonist-induced first-peak rises of $[Ca^{2+}]_i$ of platelets under conditions of Ca^{2+} entry (+$CaCl_2$) or only intracellular Ca^{2+} mobilization (+EGTA). Experiments performed as in Figs. 1-2; peak levels were reached at 75–150 s. Agonist doses 1–4 were ordered from low to high. Secondary mediator inhibitors (SMI) were present, as indicated. Peak values in nM per donor were normalized for condition of CRP 10 + $CaCl_2$ or the condition of thrombin (10 nM) + $CaCl_2$. Means ± SD (n = 3–7). All $P<0.05$ versus 100% (t-test). Raw data are presented in Suppl. Datafile 1.

Condition	Basal	Dose 1	Dose 2	Dose 3	Dose 4
CRP *(0, 1, 3, 10, 30 µg/mL)*					
$CaCl_2$	10 ± 4%	36 ± 4%	64 ± 5%	**100%**	142 ± 8%
$CaCl_2$ + SMI	8 ± 4%	29 ± 7%	46 ± 1%	59 ± 1%	64 ± 2%
EGTA	8 ± 4%	11 ± 2%	18 ± 2%	22 ± 3%	28 ± 3%
EGTA + SMI	6 ± 2%	9 ± 1%	14 ± 1%	17 ± 1%	21 ± 3%
Thrombin *(0, 0.3, 1, 3, 10 nM)*					
$CaCl_2$	10 ± 4%	20 ± 3%	35 ± 8%	57 ± 6%	**100%**
$CaCl_2$ + SMI	8 ± 4%	14 ± 1%	29 ± 1%	46 ± 10%	88 ± 3%
EGTA	8 ± 4%	13 ± 3%	19 ± 3%	26 ± 4%	39 ± 7%
EGTA + SMI	6 ± 2%	10 ± 1%	14 ± 2%	20 ± 2%	26 ± 4%

performed similar experiments employing the PAR agonists thrombin (activates PAR1 and PAR4) and TRAP (activates only PAR1). With $CaCl_2$ present, thrombin (0.3–10 nM) induced transient increases in $[Ca^{2+}]_i$, which were dose-dependent in size (Fig. 1B i). In the presence of EGTA, thrombin gave 30–50% lower peak values (Table 2), which resulted in Ca^{2+} entry ratio curves that reached a maximum of 3–4 (Fig. 1B ii-iii). Upon incubation with SMI, thrombin provoked similar $[Ca^{2+}]_i$ traces, which were only 20% lower regardless of the presence of $CaCl_2$ or EGTA (Fig. 1B iv-v). With SMI present, the overall peak values were reduced to the same extent (Table 2), while the Ca^{2+} entry ratio curves had a more transient shape (Fig. 1BA vi). Accordingly, both the individual Ca^{2+} peak values (Table 2) and the Ca^{2+} entry ratio curves pointed to a higher threshold of the thrombin dose for Ca^{2+} entry in the presence than in the absence of SMI (3 nM versus 0.3 nM).

The PAR1 agonist TRAP (0.5–15 µM) with $CaCl_2$ present evoked similar dose-dependent $[Ca^{2+}]_i$ traces as seen with thrombin, although at 25% lower peak values and an early decrease to basal level within 7 min (Suppl. Fig. 1B i). The derived Ca^{2+} entry ratio curves showed peak values of 3–4 (Suppl. Fig. 1B ii-iii). When the platelets were treated with SMI and stimulated by TRAP, the (Ca^{2+} entry ratio) curves were more transient (Suppl. Fig. 1B iv-vi). These data collectively pointed to a moderate Ca^{2+} entry ratio upon threshold levels of PAR activation, with a relatively limited contribution of secondary mediators.

3.3. Comparing of GPVI and PAR agonist effects on Ca^{2+} entry

To provide an overall comparison of the various conditions of GPVI stimulation, we compared the obtained curve parameters between experiments, and averaged these per condition (for raw data, see Datafile 1). The six curve parameters P1–6 were considered to reflect the net amounts and rates of Ca^{2+} mobilization and entry into the cytosol, under conditions of back-pumping by Ca^{2+}-ATPases in the endoplasmic reticulum and plasma menbrane. Heatmapping after univariate scaling of relevant parameter sets was then performed to make a direct comparison of the Ca^{2+} responses between agonists and doses. For CRP, the obtained heatmap indicated a stronger dose-dependent increase of all scaled parameters (except for P1) in the presence of $CaCl_2$, when compared to the EGTA condition (Fig. 2A). The $CaCl_2$-dependent effect was also apparent from the heatmapped Ca^{2+} entry ratio parameters. In the presence of SMI, parameter values of the $CaCl_2$ and Ca^{2+} entry ratio curves were reduced to half. For the weaker GPVI agonist collagen, this scaling underlined the low, both $CaCl_2$- and SMI-dependent responses (Fig. 2B).

A separate heatmap of scaled parameters for thrombin (Fig. 2C) and TRAP (Fig. 2D) demonstrated also dose-dependency, but with smaller differences between $CaCl_2$ and EGTA curves than for the GPVI agonists. A reducing effect by SMI was seen that is limited at all doses. When compared to thrombin, PAR1 stimulation with TRAP gave a similar heatmap profile, but with overall lower parameter values.Taken together, these results point to a higher reliance on Ca^{2+} entry and secondary mediators for the prolonged $[Ca^{2+}]_i$ traces induced by the GPV agonists than for traces of the PAR agonists.

3.4. Potent enforcement of GPVI-induced Ca^{2+} entry ratio by SERCA inhibition

Considering that the SERCA inhibitor thapsigargin (Table 1) stimulates Ca^{2+} entry by a continued Ca^{2+} store depletion [4], we performed a similar series of experiments by combining the GPVI or PAR agonists with an optimal dose of 1 µM thapsigargin.When combined with thapsigargin, CRP dose-dependently induced a higher increase in $[Ca^{2+}]_i$ in the presence of $CaCl_2$ and EGTA (Fig. 3A i,ii). Quantification of the $[Ca^{2+}]_i$ levels at peak time indicated a 30–150 higher increase in the presence of $CaCl_2$ (Table 2). Similarly, the Ca^{2+} entry ratio curves showed a progressive increase, reaching ratio levels as high as 300–400, hence pointing to a massively enhanced entry of Ca^{2+} (Fig. 3A iii). Of note, at very high $[Ca^{2+}]_i$ of >10 µM far above the K_d of Fura-2 of 224
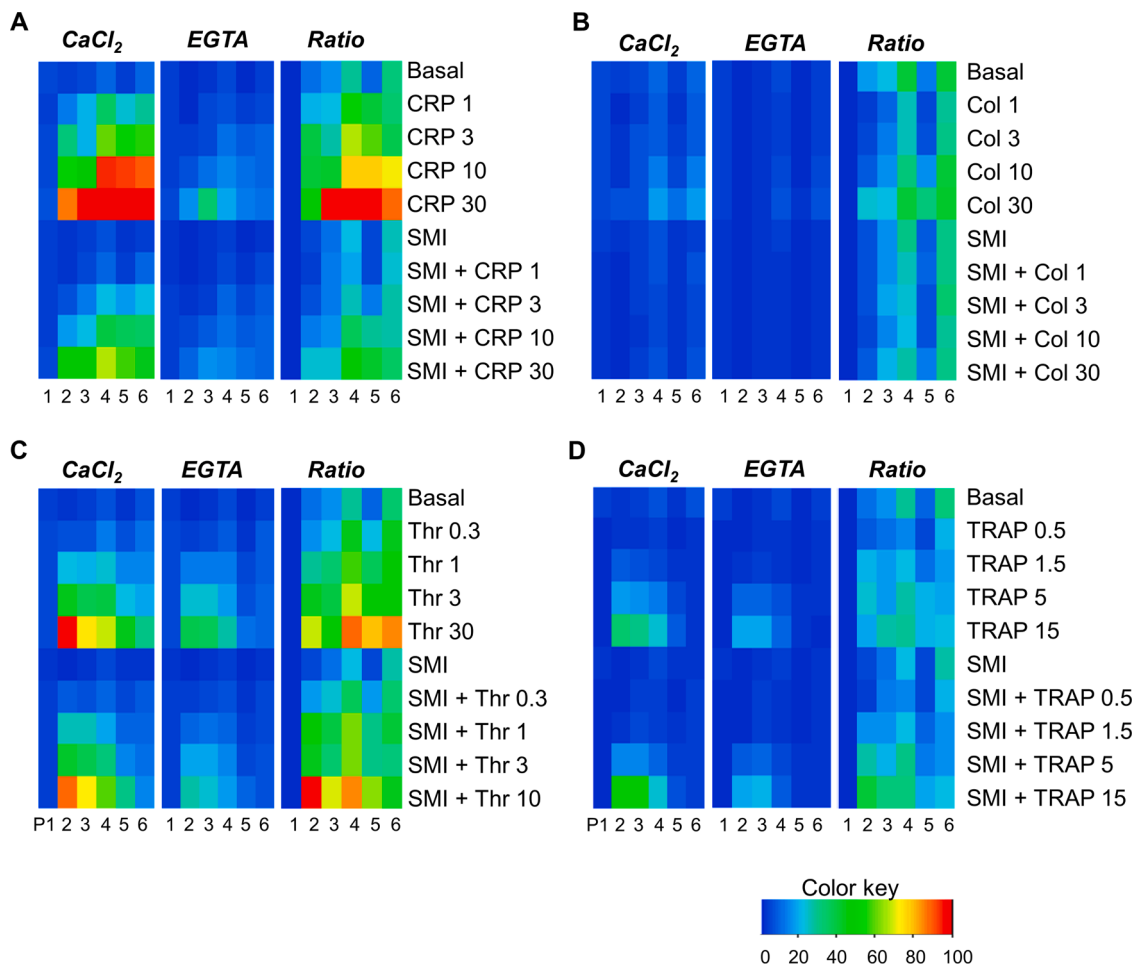
Fig. 2. Comparative dose-dependent effects on Ca²⁺ entry with collagen or thrombin receptor agonists. Fura-2-loaded platelets were stimulated with 1–30 μg/mL CRP (**A**), 1–30 μg/mL collagen (**B**), 0.3–10 nM thrombin (**C**) or 0.5–15 μM TRAP (**D**), as in (Suppl.) Fig. 1. The cells were pre-incubated with secondary mediator inhibitors (SMI), as indicated. In parallel, smoothed [Ca²⁺]$_i$ curves were generated with CaCl₂ or EGTA present, as well as Ca²⁺ entry ratio curves. Data are mean values from at least three experiments for combined CaCl₂ and EGTA conditions (*n* = 3–5 donors). Curve parameters evaluated were: level at start (P1), slope to first peak (P2), maximal change of slope (P3), maximal peak level (P4), area under the response curve over 600 s (P5), and end level after 600 s (P6). Parameters of CaCl₂ and EGTA curves were combined scaled (0–100%) in the following combinations: *(i)* P1,4,6 = nM [Ca²⁺]$_i$ values; *(ii)* P2,3 = nM/s [Ca²⁺]$_i$ slope values; and *(iii)* P5 = nM × 600 s [Ca²⁺]$_i$ integrals (P5). Separate scaling (0–100%) was performed, again using the same parameter combinations, for the Ca²⁺ entry ratio curves. Heatmaps show accordingly scaled parameters across all figure panels, to facilitate comparison of all conditions. Color key shows the scale%. For raw and scaled data, see Suppl. Datafile 1.

nM, the traces showed fluctuations caused by even minimal changes in fluorescence ratio.

When the platelets were treated with SMI, the traces with CRP + thapsigargin traces reduced 3–4 fold with CaCl₂, while those with EGTA lowered by 25% (Fig. 3A iv-v). The changes are also apparent from the quantified peak values (Table 3). With SMI, the Ca²⁺ entry ratio curves reached a lower maximum, but still reaching a value to 150 at the highest CRP dose (Fig. 3A vi).

Platelet stimulation with collagen (1–10 μg/mL) + thapsigargin (1 μM) led to higher [Ca²⁺]$_i$ traces in the presence of CaCl₂, but not of EGTA (Suppl. Fig. 2A i,ii). Of note, the highest collagen dose of 30 μg/mL gave a lower Ca²⁺ response, due to the presence of acetic acid and the pH sensitivity of the Ca²⁺ entry process [46,47]. At 10 μg/mL collagen + thapsigargin, the Ca²⁺ entry ratio curves still reached levels of 30–40 (Suppl. Fig. 2A iii). Again, the traces flattened in the presence of SMI (Suppl. Fig. 2A iv-vi). Together, these data indicate a potent enforcement of extracellular Ca²⁺ entry in GPVI-activated platelets under conditions of SERCA inhibition with thapsigargin.

3.5. Moderate enforcement of PAR-induced Ca²⁺ entry ratio by SERCA inhibition

Similar experiments were performed by activating the platelets with thapsigargin (1 μM) plus thrombin (0.3–30 nM). With CaCl₂ present this led to a dose-dependent ~2 μM peak increase in [Ca²⁺]$_i$, which was followed by a sustained [Ca²⁺]$_i$ elevation (Fig. 3B i). With EGTA present, the [Ca²⁺]$_i$ peak maximally reached 150 nM (Fig. 3B ii). The combination of thapsigargin and thrombin raised the maximal and final levels of Ca²⁺ entry ratio curves to 15 and 40, respectively (Fig. 3B iii). This pointed to a lower Ca²⁺ entry than that seen with CRP. In the presence of SMI, thrombin + thapsigargin showed similarly shaped [Ca²⁺]$_i$ traces, although amplitudes of the CaCl₂ and Ca²⁺ entry curves were lower (Fig. 3B iv-vi). This reduction, especially at lower thrombin concentrations, also appeared from the quantified peak levels (Table 3).

For platelet stimulation of TRAP plus thapsigargin, a peak increase to 2–5 μM was observed in the presence of CaCl₂, which was similar to that of thrombin (Suppl. Fig. 2B i). For traces in the presence of EGTA, amplitudes reached 90 nM, i.e. lower than with thrombin (Suppl. Fig. 2B ii). The Ca²⁺ entry ratio curves were reminiscent to those of (lower doses of) thrombin (Suppl. Fig. 2B iii). With SMI and CaCl₂ present, the [Ca²⁺]$_i$
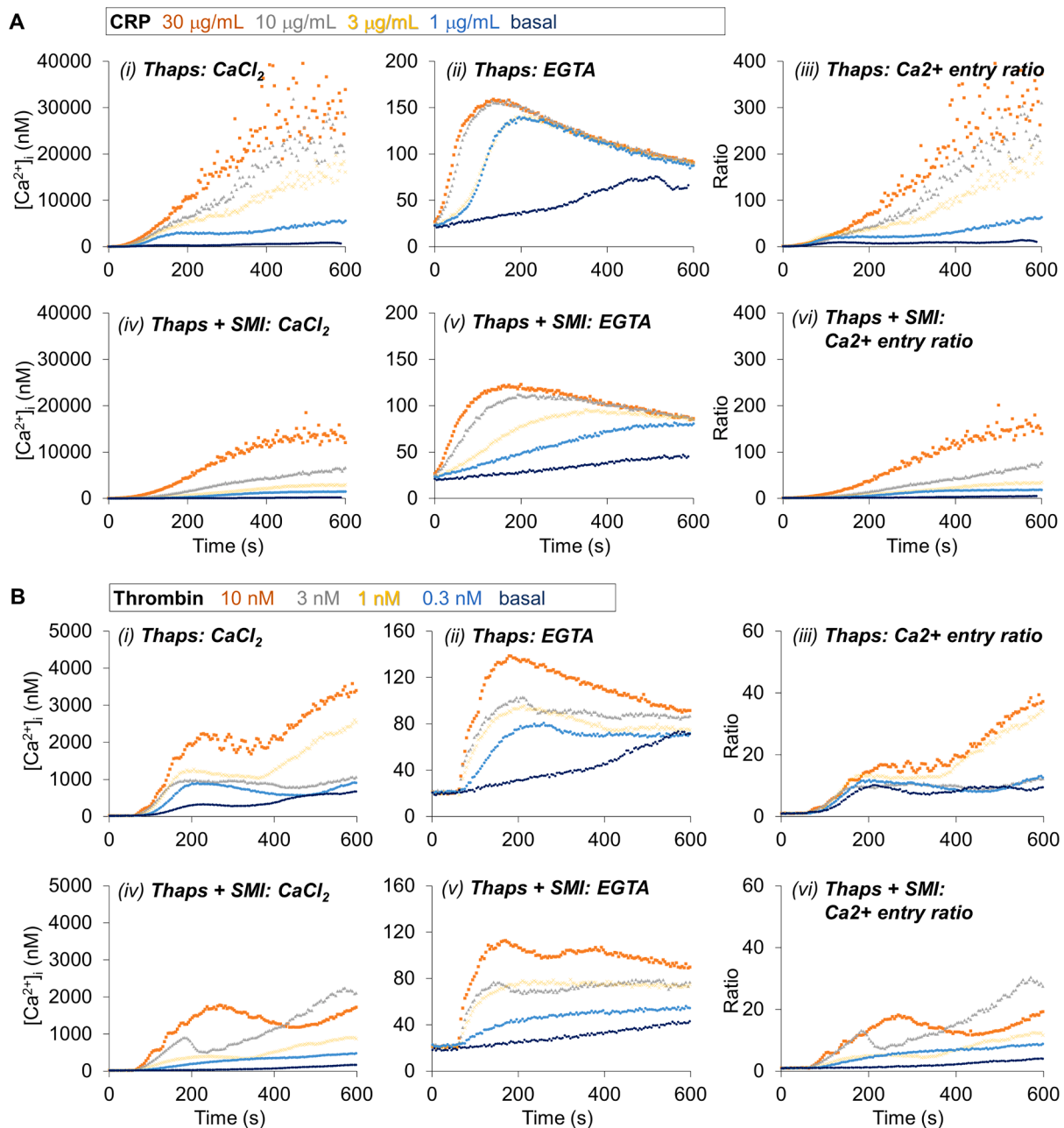
Fig. 3. Dose-dependency of Ca^{2+} entry with strong collagen or thrombin receptor agonists upon SERCA inhibition. Fura-2-loaded platelets in 96-well plates were left untreated or pre-incubated with SMI (0.1 U/mL apyrase and 20 μM indomethacin) at room temperature. Roboted stimulation in the presence of 2 mM CaCl$_2$ or 0.1 mM EGTA was with thapsigargin (1 μM) plus CRP (1–30 μg/mL) or thrombin (0.3–10 nM). Measurements of [Ca^{2+}]$_i$ were performed, as for Fig. 1. (**A-B**) Calibrated [Ca^{2+}]$_i$ traces (non-smoothed) with thapsigargin plus CRP (**A**), or thapsigargin plus thrombin (**B**), in the absence (**i-iii**) or presence (**iv-vi**) of SMI. Parallel traces were observed in the presence of CaCl$_2$ (left panels) or EGTA (middle panels). Ratio curves of Ca^{2+} entry (right panels) were obtained by dividing corresponding CaCl$_2$/EGTA curves. Data are representative of at least 3 experiments (n = 3–6 donors). For raw parameter values, see Suppl. Datafile 1.

traces of TRAP + thapsigargin though were markedly reduced, with Ca^{2+} entry ratio curves not exceeding 20 (Suppl. Fig. 2B iv-vi). Accordingly, the enforcement of thapsigargin-induced Ca^{2+} entry was lower with PAR agonists than with the strong GPVI agonist CRP.

3.6. Comparing of GPVI- and PAR-induced Ca^{2+} entry with SERCA inhibition

We also constructed heatmaps of scaled curve parameters for the four agonists (CRP, collagen, thrombin, TRAP) combined with thapsigargin in the presence of CaCl$_2$ or EGTA. The heatmaps illustrated the very potent stimulation of CRP + thapsigargin on the CaCl$_2$ curves and the

Ca^{2+} entry ratio curves, when compared to the other agonists (Fig. 4). Nevertheless, the scaled parameters of Ca^{2+} entry ratio curves for all combinations with thapsigargin showed a consistent, dose-dependent enhancement of the entry of Ca^{2+}, as well as a consistent dependency on secondary mediators. To sum up, these results point to a potent enforcement of receptor agonist-induced Ca^{2+} entry upon SERCA inhibition, which is partly dependent on secondary mediators.

3.7. Relative contribution of Ca^{2+} entry channels to GPVI- and PAR-induced Ca^{2+} entry

For investigating the comparative roles of known or presumed Ca^{2+}-

Table 3

Relative agonist-induced peak rises of $[Ca^{2+}]_i$ in the presence of thapsigargin under conditions of Ca^{2+} entry ($+CaCl_2$) or only intracellular Ca^{2+} mobilization ($+EGTA$). Experiments performed as in Figs. 1-2; peak levels of traces with EGTA were at 75–150 s, those with $CaCl_2$ at 450–500 s (CRP) or 250–300 s (thrombin). Agonist doses 1–4 were ordered from low to high, as indicated. Final thapsigargin concentration was 1 μM. Secondary mediator inhibitors (SMI) were added, where indicated. Peak values in nM per donor were normalized for the condition of CRP (10 μg/mL) + $CaCl_2$ or the condition of thrombin (10 nM) + $CaCl_2$. Means ± SD ($n = 3$–6). All $P<0.05$ versus 100%, except for *not significant (t-test). Full data are presented in Suppl. Datafile 1.

Condition	Basal	Dose 1	Dose 2	Dose 3	Dose 4
Thapsigargin + CRP *(0, 1, 3, 10, 30 μg/mL)*					
CaCl₂	3 ± 2%	23 ± 14%	56 ± 45%	**100%**	140 ± 98%*
CaCl₂ + SMI	1.0 ± 0.1%	5 ± 4%	10 ± 8%	22 ± 19%	42 ± 46%
EGTA	0.3 ± 0.1%	0.8 ± 0.3%	0.8 ± 0.3%	0.9 ± 0.3%	0.9 ± 0.3%
EGTA + SMI	0.3 ± 0.1%	0.5 ± 0.1%	0.5 ± 0.1%	0.6 ± 0.1%	0.7 ± 0.2%
Thapsigargin + thrombin *(0, 0.3, 1, 3, 10 nM)*					
CaCl₂	19 ± 8%	46 ± 24%	66 ± 35%	63 ± 29%	**100%**
CaCl₂ + SMI	6 ± 3%	22 ± 10%	34 ± 13%	71 ± 39%*	92 ± 51%*
EGTA	1.7 ± 0.8%	4.1 ± 0.3%	4.6 ± 0.4%	5.2 ± 0.5%	7.7 ± 1.3%
EGTA + SMI	1.5 ± 0.4%	3.1 ± 0.8%	3.7 ± 0.3%	4.5 ± 0.8%	5.6 ± 0.5%

permeable cation channels or transporters in the Ca^{2+} entry process, we used a panel of pharmacological inhibitors. Table 1 gives the targets and commonly used concentrations of the used inhibitors in platelet research. The compound 2-ABP was used a blocker of the STIM1-coupled ORAI1 channel, although it also affects the InsP₃-induced Ca^{2+} mobilization [48,49]. For comparison, we used the ORAI channel blocker Synta66 [49], and also the STIM1 inhibitor ML-9 (also blocking MLCK and Akt isoforms) [50]. Earlier dose-response curves with human platelets showed a more selective inhibitory effect of Synta66 than 2-APB on SOCE in comparison to intracellular Ca^{2+} mobilization [49]. Other aspecific effects are not commonly described [51]

To block the most abundantly expressed TRPC isoform, TRPC6, we used the compound BI-749,327 [52], which has recently been used as a specific TRPC6 inhibitor to improve platelet preservation upon storage [53]. Furthermore, the mechanosensitive Piezo1/2 ion channels were blocked with the compound GsMTx4 [31]. In human platelets, GsMTx4 (micromolar range) was shown not to affect Ca^{2+} influx via ORAI1 or TRPC6 channels [54].

As a most specific antagonist of ATP-induced Ca^{2+} entry via P2×₁ channels, we tested MRS-2159 [55,56]. Furthemore, for blockage of the NCX3 Na^{+}/Ca^{2+} exchanger, we used the compound ORM-10,103. In oher cells types this has been described as a specific inhibitor of NCX and ʟ-type Ca^{2+} currents in the 3–10 μM dose range [57]. For human platelets, dosing of ORM-10,103 indicated a IC_{50} of ~10 μM on the Ca^{2+}-dependent procoagulant activity induced by GPVI and PAR stimulation [32].

Although almost all of these compounds have been used in the 1–10 μM range, we first performed a 1–30 μM dose-response experiment using the standard agonist concentrations of CRP (10 μg/mL) or thrombin (10 nM). By comparing the $CaCl_2$ and EGTA curves, the largest $[Ca^{2+}]_i$ altering effects (if any) of 2-APB, BI-749,327, ORM-10,103 and Synta66 were obtained at 30 μM, while of ML-9 and MRS-21,593 these were reached at 10 μM (not shown). Since for GsMTx4 no clear effects were observed, this compound was discarded. Accordingly, these concentrations were chosen for further experiments.

In a large set of experiments, the six compounds were systematically tested for effects on CRP- or thrombin-induced $[Ca^{2+}]_i$ traces in $CaCl_2$ or EGTA medium, also using the modifying conditions with SMI and/or

thapsigargin present. The resulting, representative Ca^{2+} entry ratio traces showed for 2-ABP a potent suppression with either agonist (Fig. 5A); for BI-749,327 no more than small effects (Fig. 5B); for MRS-2159 small reductions in the first part of the curves (Fig. 5C); for ORM-10,103 longer-term reductions (Fig. 5D); and for Synta66 a continued inhibition (Fig. 5E).

For all inhibitor experiments, we determined the curve parameters (P1–6) in the presence of $CaCl_2$ or EGTA, as well as from the calculated Ca^{2+} entry ratio traces. To assess the inhibitor effects on the Ca^{2+} entry process, we used two approaches: a calculation of effects per parameter and curve type, and a calculation of relative effects per parameter on $CaCl_2$ curves ratioed to EGTA curves. Upon CRP stimulation, heatmapping of the effects on Ca^{2+} entry ratio curves and on relative effect parameters indicated a strong, significant inhibition for all Ca^{2+} entry parameters (2×5) with 2-APB, which remained in the presence of SMI (Fig. 6A). For Synta66 and ORM-10,103, most of the Ca^{2+} entry parameters showed a less strong, but still significant inhibition. With MRS-2159, only the initial parameter P2 (slope to first peak) was lowered. With BI-749,317 or ML-9 the Ca^{2+} entry parameters did not decrease or rather increased.

In comparison, upon thrombin stimulation without or with SMI (Fig. 6B), heatmapping showed with 2-APB again a strong and significant reduction in all C^{a2+} entry parameters. The effects of Synta66 and ORM-10,103, while mostly significant, were smaller in size. MRS-2159 again affected only parameter P2. While BI-749,317 was without effect, ML-9 increased some parameter values although of no significance.

For the inhibitors with largest effect sizes upon thrombin stimulation (PAR1+4), we also compared the effects on Ca^{2+} entry curve parameters in response to peptide stimulation of PAR1 (TRAP), PAR4 (AYPGKF) or the combination of PAR1+4 (TRAP + AYPGKF). As shown in Suppl. Fig. 3, we found similar size effects on the Ca^{2+} entry parameters upon PAR1 and/or PAR4 stimulation, Heatmap presentation indicated that, regardless of the agonist used (thrombin TRAP, AYPGKF, TRAP+AYPGKF), suppressive effects of 2-ABP were larger than those of ORM-10,103.

Similar heatmaps were generated for the assessment of inhibitor effects in platelets stimulated with CRP or thrombin in the presence of thapsigargin. Representative Ca^{2+} entry ratio curves indicate a potent, almost abolishing effect of 2-APB on the entry process with either agonist combination (Fig. 7A-B). This reduction was also apparent from generated heatmaps, which for CRP + thapsigargin showed strong and significant reducing effects of 2-APB and Synta66 on all Ca^{2+} entry parameters (Fig. 7C). This reduction remained in the presence of SMI. For thrombin + thapsigargin, again strongly reducing effects of 2-APB and Synta66 were obtained (Fig. 7D). Furthermore, for either agonist combination, also ORM-10,103 showed a significant inhibitory profile on most Ca^{2+} entry parameters, although of a greater effect size with thrombin than with CRP (Fig. 7C-D). Regarding the other inhibitors, BI-749,427 and ML-9 tended to increase rather than decrease a subset of parameters, whereas MRS-2159 was essentially without effect. Altogether, these data point, for the collagen and thrombin receptor agonists, to an inhibitory effect on Ca^{2+} entry in the order of 2-APB > Synta66 (strongest with thapsigargin) > ORM-10,103 > MRS-2159 (initial parameter) >BI-749,327, ML-9.

4. Discussion

In this paper, we employed a high-throughput assay with Fura-2-loaded platelets, for obtaining sets of calibrated agonist-induced $[Ca^{2+}]_i$ traces in the presence of either extracellular $CaCl_2$ or EGTA. As reviewed earlier [1,4], these traces were assumed to reflect the summation of Ca^{2+} fluxes by InsP₃-induced Ca^{2+} mobilization from stores and Ca^{2+} entry mechanisms, restrained by a backpumping of mobilized Ca^{2+} by SERCA and PMCA isoforms. Of note, when observed per individual platelet, the Ca^{2+} fluxes are higher than currently measured, as the steeply spiking Ca^{2+} transients in platelet suspensions
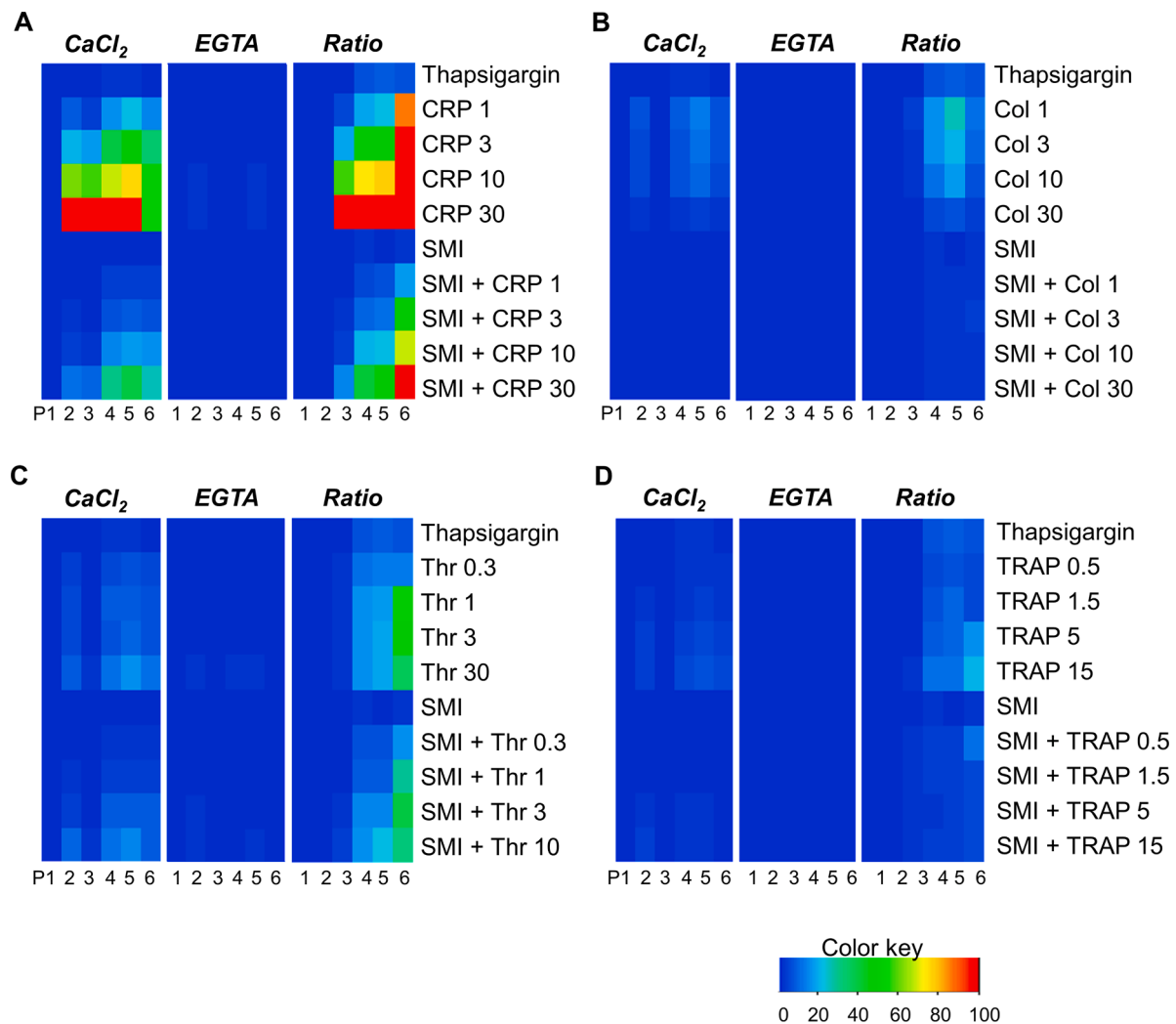
Fig. 4. Comparative dose-dependent effects on Ca^{2+} entry with collagen or thrombin receptor agonists upon SERCA inhibition. Fura-2-loaded platelets in the presence of 2 mM CaCl$_2$ or 0.1 mM EGTA were stimulated with 1–30 μg/mL CRP (**A**), 1–30 μg/mL collagen (**B**), 0.3–10 nM thrombin (**C**) or 0.5–15 μM TRAP (**D**), as in (Suppl.) Fig. 3. In all conditions, thapsigargin (1 μM) was added to the agonist mixture. The cells were pre-incubated with secondary mediator inhibitors (SMI), as indicated. Parallel [Ca^{2+}]$_i$ curves were generated with CaCl$_2$ or EGTA present, as well as derived Ca^{2+} entry ratio curves. Data are mean values from at least three experiments for combined CaCl$_2$ and EGTA conditions (*n* = 3–5 donors). Curve parameters evaluated were: level at start (P1), slope to first peak (P2), maximal change of slope (P3), maximal peak level (P4), area under the response curve over 600 s (P5), and end level after 600 s (P6). Parameters of CaCl$_2$ and EGTA curves were combined scaled (0–100%) in the following combinations: *(i)* P1,4,6 = nM [Ca^{2+}]$_i$ values; *(ii)* P2,3 = nM/s [Ca^{2+}]$_i$ slope values; and *(iii)* P5 = nM × 600 s [Ca^{2+}]$_i$ integrals (P5). Separate scaling (0–100%) was performed, again using the same parameter combinations, for the Ca^{2+} entry ratio curves. Heatmaps show accordingly scaled curve parameters across all figure panels, thus to facilitate comparison of all conditions. Color key shows the scale%. For raw and scaled data, see Suppl. Datafile 1.

are averaged out [16]. By considering that the traces with CaCl$_2$ result from the addition of Ca^{2+} entry to the traces with EGTA, we constructed sets of Ca^{2+} entry ratio curves, which provide a quantitative indication of the size over time of the Ca^{2+} entry process.

In our calculations of Ca^{2+} fluxes, due to lack of quantitative affinity and expression data, we did not separate out Ca^{2+} uptake by the mitochondrial calcium uniporter [58] or by Ca^{2+}-induced Ca^{2+} release via the mitochondrial permeability transition pore [9,15]. However, for mouse platelets it was established that mitochondrial uniporters do take up Ca^{2+} ions in activated platelets [58], whereas the mitochondrial permeability transition pore mostly in highly activated, procoagulant platelets contributes to persistently high, entry-dependent [Ca^{2+}]$_i$ levels [9,15].

The constructed Ca^{2+} entry ratio curves indicated for strong platelet agonists, i.e. CRP (GPVI ligand) and thrombin (PAR1/4 ligand), a 3–7 fold enhanced Ca^{2+} entry, when added above threshold doses, while these levels were lower upon inhibition of the secondary mediators ADP

and thromboxane A$_2$. On the other handn, the weaker agonists collagen (for GPVI) and TRAP (for PAR1) triggered a moderately enhanced Ca^{2+} entry, which again depended on secondary mediator release. Strikingly, by combining the agonists with the SERCA inhibitor thapsigargin, we observed a dramaticlly increased Ca^{2+} entry, with ratio levels reaching 400 (with CRP) or 40 (with thrombin). These values suggest a better degree of coupling of SOCE to Ca^{2+} store depletion in response to GPVI than to PAR stimulation. A high level of SOCE in human or mouse platelets was also previously seen with the GPVI agonist convulxin [19, 49]. A novel finding is that also in the presence of thapsigargin the high Ca^{2+} entry greatly relied on platelet co-activation by secondary mediators. Together, these data indicate that the approach of calculating Ca^{2+} entry ratios can provide novel and relevant information on the agonist-induced Ca^{2+} entry, and by extension to the platelet activation process.

Regarding the net Ca^{2+} fluxes in platelets, we obtained a maximal Ca^{2+} mobilization with CRP and thapsigargin in the presence of EGTA of
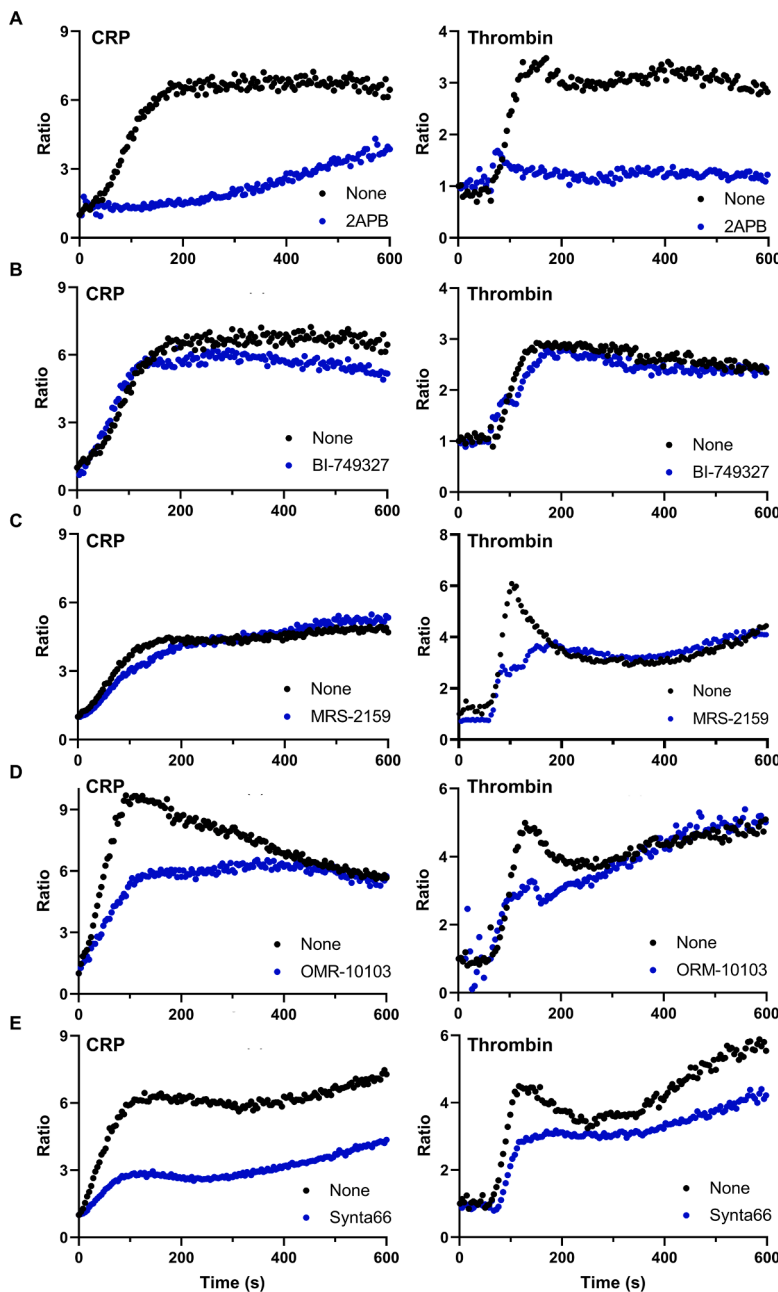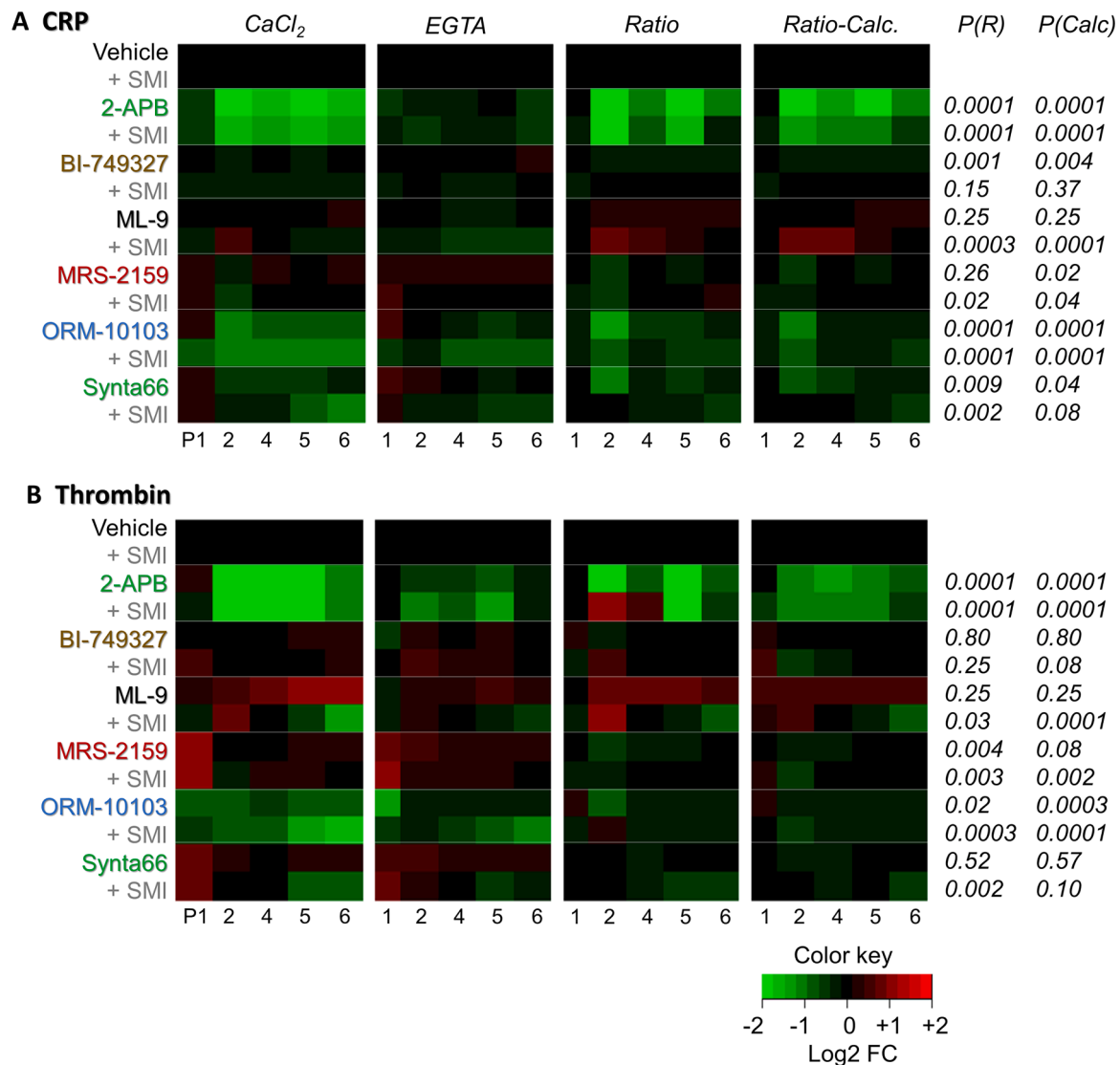
Fig. 5. Effects of pharmacological inhibitors on Ca²⁺ entry with collagen or thrombin receptor agonists. Fura-2-loaded platelets in the presence of 2 mM CaCl₂ or 0.1 mM EGTA were stimulated with 10 µg/mL CRP (left panels) or 10 nM thrombin (right panels) after pre-incubation with vehicle solution (none) or indicated inhibitor at room temperature. Final concentrations were as follows: 2-APB (30 µM), BI-749,327 (30 µM), ML-9 (not shown, 10 µM), MRS-2159 (10 µM), ORM-10,103 (30 µM) and Synta66 (30 µM). Parallel [Ca²⁺]ᵢ curves generated with CaCl₂ or EGTA during 600 s were converted into Ca²⁺ entry ratio curves. Shown are representative Ca²⁺ entry ratio curves for *n* = 3–5 independent experiments. For raw values, see Suppl. Datafile 2.

150 nM [Ca²⁺]ᵢ. Based on a mean cytosolic volume of platelet of 8.92 fL (see methods), this points to a net estimate of 5.37 × 150 = 805 mobilizable Ca²⁺ ions from stores per single platelet. With CaCl₂ present, this net Ca²⁺ entry can raise up to 400-fold higher. For these calculations it should be noted that these do not take into account inter-individual variation in platelet Ca²⁺ signaling [35,59,60], nor intra-individual differences between platelet populations [39,61], and neither effects of combinations of agonists [62,63].

Table 4 summarizes the overall effects of the various pharmacological inhibitors on extracellular Ca²⁺ entry and intracellular Ca²⁺ mobilization. The consistent inhibition of Ca²⁺ entry with 2-APB (50–80%) and Synta66 (15–80%) point to ORAI1 as a main Ca²⁺ channel regulating GPVI- and PAR-induced Ca²⁺ entry in the presence of thapsigargin. The difference between 2-APB and Synta66 can be explained by an additional, known inhibitory effect of 2-APB, but not Synta66, on Ca²⁺ store depletion [48,64]. This also suggests a certain degree of synergy between both processes, e.g. via the mechanism of

Ca²⁺-induced Ca²⁺ release. Confirming evidence for a major role of the ORAI1-STIM1 pathway indeed comes from patients with a homozygous R91W mutation in ORAI1 or an R429C mutation in STIM1, where in platelets the thapsigargin-mediated Ca²⁺ entry was fully annulled [24]. Interestingly, the Ca²⁺ entry after convulxin stimulation was stronger impaired with the ORAI1 mutation than with the STIM1 mutation [24], pointing to a more crucial role of the ORAI1 channel activity. This may also be concluded from the absence of inhibitory effects (rather a tendency to stimulation) of the STIM1 inhibitor ML-9, with the note that it also targets MLCK and Akt isoforms (Table 1). In human platelets, the isoforms ORAI2/ORAI3 and STIM2 are expressed at no more than low levels [65].

Table 4 furthermore summarizes that the TRPC6 inhibitor BI-749,327 [52] at the dose applied failed to suppress Ca²⁺ entry. In line with this finding, for mouse platelets, the role of TRPC6 was found to rely on ORAI1 activity [30]. We note here that we did not study the oleoyl-acetyl glycerol-induced Ca²⁺ entry, which pathway requires

Fig. 6. Combined effects of pharmacological inhibitors on Ca^{2+} entry with collagen or thrombin receptor agonists. Fura-2-loaded platelets in the presence of 2 mM CaCl$_2$ or 0.1 mM EGTA were stimulated with CRP (**A**) or thrombin (**B**) after pre-incubation with vehicle solution or indicated channel inhibitor. Secondary mediator inhibitors (SMI, indomethacin and apyrase) were added, where indicated. Final concentrations were as in Fig. 5: 2-APB (30 μM), BI-749,327 (30 μM), ML-9 (10 μM), MRS-2159 (10 μM), ORM-10,103 (30 μM) or Synta66 (30 μM). Parallel [Ca^{2+}]$_i$ curves generated with CaCl$_2$ or EGTA used for the construction of Ca^{2+} entry ratio curves. Parameters per curve then analyzed were: level at start (P1), slope to first peak (P2), maximal peak level (P4), area under the response curve (P5), and level at end (P6). Inhibitor effects (compared to vehicle) were calculated per experiment, curve type and parameter. In addition, the ratios of inhibitor effects on CaCl$_2$ versus EGTA curves were calculated (Ratio-Calc.). Heatmaps show the mean log2 fold changes (FC) of inhibitor effects per curve and parameter versus the vehicle-control condition. Green = decrease, red = increase. Data are for n = 3–5 donors. P values of combined parameters vs. control condition are indicated for Ca^{2+} entry ratio curves = $P(R)$ and for Ratio-Calc. curves = $P(Calc)$ (repetitive t-test). For raw values, see Suppl. Datafile 2.

TRPC6 activity [28,29].

In platelets, the ATP-induced P2X$_1$ Ca^{2+} channel is an early onset which is rapidly desensitized by its ligand [26,27]. Using the inhibitor MRS-2159, our data also point to an only early contribution of P2X$_1$ in the Ca^{2+} entry process (i.e. parameter P2). However, in our experiments with washed platelets, we may not have fully prevented desensitization of the channel. On the other hand, due to autocrine ATP release, P2X$_1$ desensitization will already occur in the beginning of the 10-min Ca^{2+} responses.

Platelet Na$^+$/Ca^{2+} exchangers (NCEs), operating in reverse mode have been shown to contribute to the prolongedly high [Ca^{2+}]$_i$ required for the formation of procoagulant platelets, such as measured with the probe annexin A5 [32]. Our experiments with ORM-10,103 point to a partial inhibition (20–60%) of Ca^{2+} entry, along with a smaller effect on Ca^{2+} mobilization (Table 4). Human platelets express five Na$^+$/Ca^{2+} exchangers (genes *SLC8A1,3* and *SLC24A1,3,4*) [65]. The compound

ORM-10,103 is primarily directed to NCX3 (*SLC8A3*). To which extent the other isoforms contribute to the regulation of Ca^{2+} fluxes is still unclear. Collectively, our data thus reveal ORAI1 and NCE as the dominating Ca^{2+} transporters regulating the long-term GPVI- and PAR-induced Ca^{2+} entry in human platelets.

For essentially all agonists and combinations, we found reducing effects on the various (ratioed) [Ca^{2+}]$_i$ traces in the presence of SMI, blocking the autocrine effects of released ADP and thromboxane A$_2$ (Figs. 2, 4). This agrees with a reference paper reporting on the major contributions of these feedback mediators to platelet aggregation and secretion in response to GPVI or PAR agonists, sch as measured by light transmission aggregometry [66].

This study provides novel information on platelet Ca^{2+} signaling, but also has some limitations. First, our data provide newquantitative insight into the key importance of the ORAI1-STIM1 Ca^{2+} entry pathway for platelet activation, such in agreement with the impaired thrombus
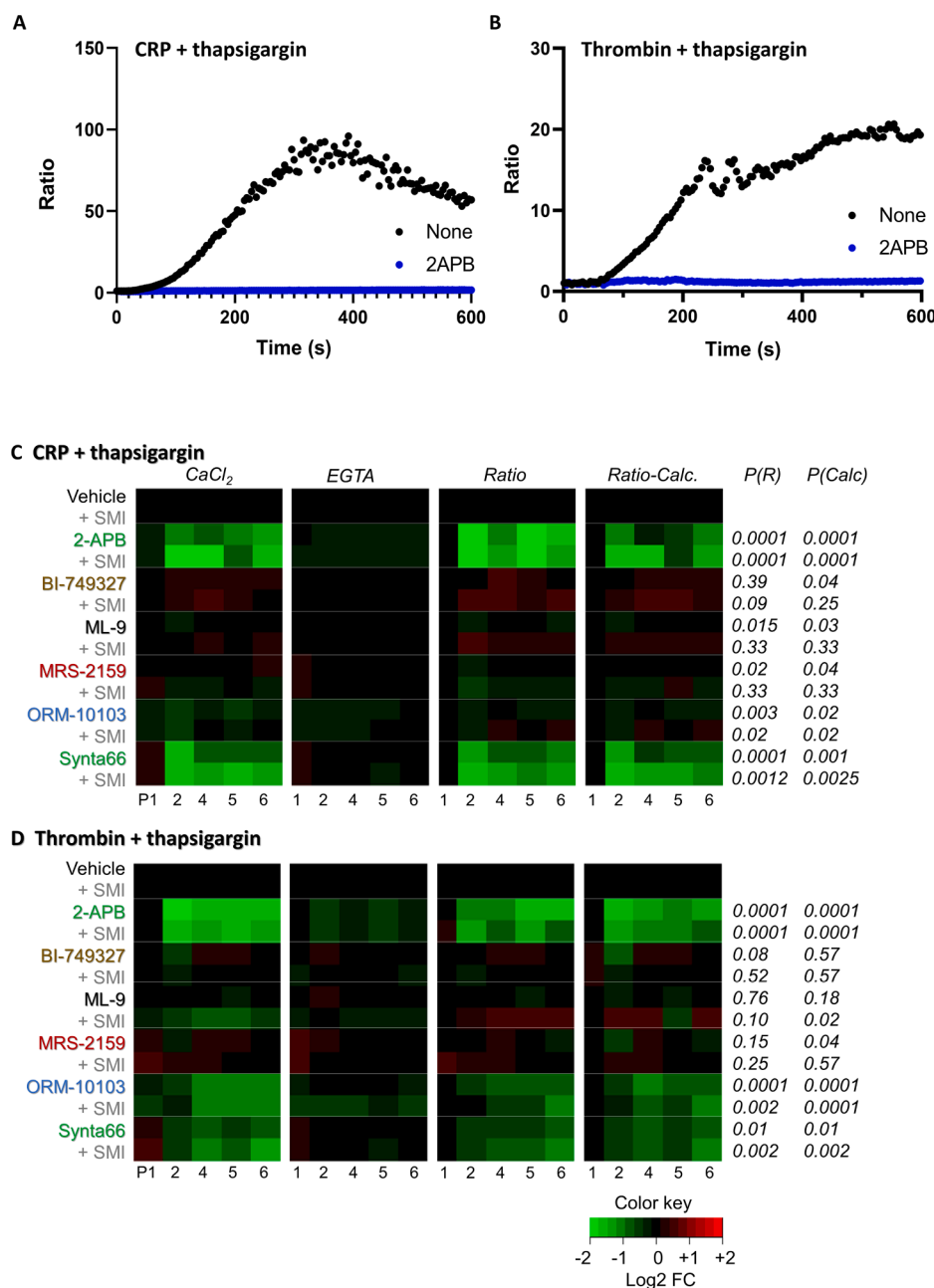
Fig. 7. Combined effects of pharmacological inhibitors on Ca^{2+} entry by collagen and thrombin receptor agonists upon SERCA inhibition. Inhibitor experiments with Fura-2-loaded platelets were performed as for Fig. 6, but additionally thapsigargin (1 μM) was added as agonist together with CRP (**A, C**) or thrombin (**B, D**). Effects on parameters of CaCl$_2$, EGTA, Ca^{2+} entry ratio and calculated ratios (Ratio-Calc.) were also obtained as for Fig. 6. Shown are representative Ca^{2+} entry ratio curves for 2-ABP (**A, B**). Furthermore, heatmaps of mean log2 fold changes (FC) of inhibitor effects per curve and parameter vs. the vehicle-control condition (**C, D**). Green = decrease, red = increase. Data are for n = 3–5 donors. *P* values of combined parameters vs. control condition are indicated for Ca^{2+} entry ratio curves = *P (R)* and for Ratio-Calc. curves = *P(Calc)* (repetitive *t*-test). For raw values, see Suppl. Datafile 2.

formation reported mice or patients with a genetic ORAI1 or STIM1 dysfunction [19,22,24]. Hence, pharmacological targeting of the ORAI1 channel may be an interesting approach to treat arterial thrombosis, although it should be remarked that complete abrogation of the channel activity associates with immune deficiency [4,14]. Also new is our evidence for a general role of NCE isoforms in Ca^{2+} signaling, thus taking further the recognition that these ion transporters are involved in the Ca^{2+} elevation preceding procoagulant platelet formation [32]. The OMIM database of human genetics only reports on night blindness in carriers of an *SLC24A1* mutation and on pigmentation abnormalities linked to *SLC24A4* mutations [67]. The NCE channel types may thus be interesting and novel drug targets. Third, the observed effects of ORAI1 or NCE inhibition in the presence of SMI (inhibiting cyclooxygenase and ADP receptors) suggests that those drugs affecting ORAI1 or NCEs will be effective on top of the current antiplatelet agents, aspirin and P2Y$_{12}$ inhibitors. A limitation of our approach - high throughput screening setup to define and quantify Ca^{2+} entry mechanisms - is that the

multitude of assay variables did not allow simultaneous measurements of other functional responses of platelets. For the functional relevance of the Ca^{2+} entry process we like to refer to papers using flow cytometric or microfluidic approaches. For instance, the blockage ORAI1 in human platelets with 2-APB or Synta66 has been shown to suppress collagen-induced thrombus formation and annexin A5 binding (phosphatidylserine expression) [49]. A second limitation is that we considered the intracellular Ca^{2+} stores of platelets as one compartment, not taking into account separate Ca^{2+} uptake or release from mitochondria or lysosomes. Reason for this is that the Ca^{2+} fluxes in these organelles were not easy to assess. Third, the followed pharmacological approach to quantify Ca^{2+} entry fluxes in platelets implies a certain degree of dose-dependent non-specificity of the inhibitors used. Additional preclinical studies will be needed to show the suitability of the compounds and their targets in the field of thrombosis and hemostasis.

Table 4
Relative effects of inhibitors on CRP- or thrombin-induced Ca²⁺ entry and Ca²⁺ mobilization. Presence of SMI and/or thapsigargin (thaps.) is as indicated. Mean (SD) effects of inhibitors on parameters (P2,4–6) of Ca²⁺ ratio and EGTA curves. Relevant inhibition (≥15%) is indicated in italic & underlining.

Condition	Ca²⁺ entry				Ca²⁺ mobilization			
	- SMI	+ SMI	- SMI + thaps.	+ SMI + thaps.	- SMI	+ SMI	- SMI + thaps.	+ SMI + thaps.
CRP								
2-APB (ORAI1, IP3R)	*0.36 (0.13)*	*0.49 (0.19)*	*0.28 (0.26)*	*0.18 (0.16)*	*0.83 (0.10)*	*0.76 (0.07)*	*0.70 (0.05)*	*0.76 (0.04)*
Synta66 (ORAI1)	*0.70 (0.11)*	*0.85 (0.10)*	*0.29 (0.10)*	*0.16 (0.04)*	1.01 (0.09)	*0.76 (0.08)*	0.95 (0.04)	0.89 (0.06)
BI-749,327 (TRPC6)	*0.85 (0.05)*	1.02 (0.04)	1.41 (0.29)	1.98 (0.54)	1.05 (0.06)	0.91 (0.02)	1.00 (0.06)	0.94 (0.02)
ML-9 (STIM1, Akt)	1.11 (0.04)	1.43 (0.33)	0.87 (0.12)	1.52 (0.15)	0.90 (0.09)	*0.73 (0.05)*	1.00 (0.02)	0.89 (0.00)
MRS-2159 (P2 × 1)	0.87 (0.12)	0.94 (0.12)	0.96 (0.15)	*0.75 (0.25)*	1.21 (0.03)	0.97 (0.06)	1.03 (0.04)	0.97 (0.03)
ORM-10,103 (NCE)	*0.68 (0.17)*	*0.72 (0.08)*	*0.75 (0.12)*	1.08 (0.34)	*0.82 (0.11)*	*0.66 (0.11)*	*0.82 (0.04)*	*0.83 (0.01)*
Thrombin								
2-APB (ORAI1, IP3R)	*0.46 (0.15)*	*0.64 (0.39)*	*0.16 (0.05)*	*0.23 (0.07)*	*0.66 (0.13)*	*0.60 (0.18)*	*0.59 (0.11)*	*0.59 (0.09)*
Synta66 (ORAI1)	0.92 (0.07)	0.86 (0.15)	*0.45 (0.07)*	*0.35 (0.13)*	1.30 (0.14)	0.90 (0.22)	0.98 (0.08)	0.91 (0.10)
BI-749,327 (TRPC6)	0.97 (0.08)	1.00 (0.17)	1.20 (0.46)	1.01 (0.20)	1.12 (0.04)	1.15 (0.14)	1.07 (0.12)	0.94 (0.16)
ML-9 (STIM1, Akt)	1.57 (0.16)	0.91 (0.26)	0.88 (0.12)	1.95 (0.86)	1.24 (0.07)	0.92 (0.22)	1.12 (0.12)	*0.73 (0.11)*
MRS-2159 (P2 × 1)	0.87 (0.11)	0.91 (0.12)	0.96 (0.28)	1.23 (0.19)	1.26 (0.06)	1.16 (0.12)	1.19 (0.18)	1.02 (0.10)
ORM-10,103 (NCE)	*0.78* (0.09)	*0.83* (0.12)	*0.35 (0.10)*	*0.48 (0.23)*	*0.78* (0.01)	*0.64* (0.18)	0.89 (0.11)	*0.52* (0.06)

CRediT authorship contribution statement

Hilaire Yam Fung Cheung: Conceptualization, Data curation, Formal analysis, Writing – original draft, Writing – review & editing. **Jinmi Zou:** Conceptualization, Data curation, Formal analysis, Writing – original draft, Writing – review & editing. **Chukiat Tantiwong:** Investigation, Methodology, Validation, Writing – review & editing. **Delia I. Fernandez:** Investigation, Methodology, Validation, Writing – review & editing. **Jingnan Huang:** Investigation, Methodology, Validation, Writing – review & editing. **Robert Ahrends:** Funding acquisition, Supervision, Writing – review & editing. **Mark Roest:** Funding acquisition, Supervision, Writing – review & editing. **Rachel Cavill:** Investigation, Methodology, Validation, Writing – review & editing. **Jon Gibbins:** Funding acquisition, Supervision, Writing – review & editing. **Johan W. M. Heemskerk:** Funding acquisition, Supervision, Writing – original draft, Writing – review & editing.

Declaration of Competing Interest

MR is an employee of Synapse Research Institute. JWMH is a scientific advisor of Synapse Research Institute. The other authors report no relevant conflicts of interest.

Data availability

Data will be made available on request.

Supplementary materials

Supplementary material associated with this article can be found, in the online version, at doi:10.1016/j.ceca.2023.102738.

References

[1] J.W. Heemskerk, Calcium and platelets, in: R Pochet, R Donato, J Haiech, C Heinzmann, V Gerke (Eds.), The Molecular Basis of Calcium Action in Biology and Medicine, Kluwer Acad. Publ., The Hague (the Netherlands), 2000, pp. 45–71, pages.

[2] D. Varga-Szabo, A. Braun, B. Nieswandt, Calcium signaling in platelets, J. Thromb. Haemost. 7 (2009) 1057–1066.

[3] H.H. Versteeg, J.W. Heemskerk, M. Levi, P.H. Reitsma, New fundamentals in hemostasis, Physiol. Rev. 93 (2013) 327–358.

[4] E. Mammadova-Bach, M. Nagy, J.W. Heemskerk, B. Nieswandt, A. Braun, Store-operated calcium entry in thrombosis and thrombo-inflammation, Cell Calcium 77 (2019) 39–48.

[5] F.A. Solari, N.J. Mattheij, J.M. Burkhart, F. Swieringa, P.W. Collins, J. M. Cosemans, A. Sickmann, J.W. Heemskerk, R.P. Zahedi, Combined quantification of the global proteome, phosphoproteome, and proteolytic cleavage to characterize altered platelet functions in the human Scott syndrome, Mol. Cell. Proteomics. 15 (2016) 3154–3169.

[6] F. Beck, J. Geiger, S. Gambaryan, F.A. Solari, M. Dell'Aica, S. Loroch, N. Mattheij, I. Mindukshev, O. Pötz, K. Jurk, J.M. Burkhart, C. Fufezan, J.W. Heemskerk, U. Walter, R.P. Zahedi, A. Sickmann, Temporal quantitative phosphoproteomics of ADP stimulation reveals novel central nodes in platelet activation and inhibition, Blood 129 (2017) e1–e12.

[7] H.Y. Cheung, C. Coman, P. Westhoff, M. Manke, A. Sickmann, O. Borst, M. Gawaz, S.P. Watson, J.W. Heemskerk, R. Ahrends, Targeted phosphoinositides analysis using high-performance ion chromatography-coupled selected reaction monitoring mass spectrometry, J. Proteome Res. 20 (2021) 3114–3123.

[8] J. Wu, J.W. Heemskerk, C.C. Baaten, Platelet membrane receptor proteolysis: implications for platelet function, Front. Cardiovasc. Med. 7 (2021), 608391.

[9] D.I. Fernandez, M.J. Kuijpers, J.W. Heemskerk, Platelet calcium signaling by G-protein coupled and ITAM-linked receptors regulating anoctamin-6 and procoagulant activity, Platelets 32 (2021) 863–871.

[10] P.E. Van der Meijden, J.W. Heemskerk, Platelet biology and functions: new concepts and clinical perspectives, Nat. Rev. Cardiol. 16 (2019) 166–179.

[11] S.P. Watson, J.M. Auger, O.J. McCarty, A.C. Pearce, GPVI and integrin aIIbb3 signaling in platelets, J. Thromb. Haemost. 3 (2005) 1752–1762.

[12] S. Offermanns, Activation of platelet function through G protein-coupled receptors, Circ. Res. 99 (2006) 1293–1304.

[13] G. De Gaetano, C. Cerletti, E. Dejana, R. Latini, Pharmacology of platelet inhibition in humans: implications of the salicylate-aspirin interaction, Circulation 72 (1985) 1185–1193.

[14] S. Feske, Y. Gwack, M. Prakriya, S. Srikanth, S.H. Puppel, B. Tanasa, P.G. Hogan, R. S. Lewis, M. Daly, A.K. Rao, A mutation in Orai1 causes immune deficiency by abrogating CRAC channel function, Nature 441 (2006) 179–185.

[15] F. Lang, P. Münzer, M. Gawaz, O. Borst, Regulation of STIM1/Orai1-dependent Ca²⁺ signalling in platelets, Thromb. Haemost. 110 (2013) 925–930.

[16] J.W. Heemskerk, P. Vis, M.A. Feijge, J. Hoyland, W.T. Mason, S.O. Sage, Roles of phospholipase C and Ca²⁺-ATPase in calcium responses of single, fibrinogen-bound platelets, J. Biol. Chem. 268 (1993) 356–363.

[17] M. Prakriya, S. Feske, Y. Gwack, S. Srikanth, A. Rao, P.G. Hogan, Orai1 is an essential pore subunit of the CRAC channel, Nature 443 (2006) 230–233.

[18] R.M. Luik, B. Wang, M. Prakriya, M. Wu, R.S. Lewis, Oligomerization of STIM1 couples ER calcium depletion to CRAC channel activation, Nature 454 (2008) 538–542.

[19] D. Varga-Szabo, A. Braun, B. Nieswandt, STIM1 and Orai1 in platelet function, Cell Calcium 50 (2011) 70–278.

[20] J. Volz, C. Kusch, S. Beck, M. Popp, T. Vögtle, M. Meub, I. Scheller, H.S. Heil, J. Preu, M.K. Schuhmann, K. Hemmen, T. Premsler, A. Sickmann, K.G. Heinze, D. Stegner, G. Stoll, A. Braun, M. Sauer, B. Nieswandt, BIN2 orchestrates platelet

calcium signaling in thrombosis and thrombo-inflammation, J. Clin. Invest. 130 (2020) 6064–6079.

[21] W. Bergmeier, M. Oh-hora, C.A. McCarl, R.C. Roden, P.F. Bray, S. Feske, R93W mutation in Orai1 causes impaired calcium calcium influx in platelets, Blood 109 (2009) 6875–6878.

[22] A. Braun, D. Varga-Szabo, C. Kleinschnitz, I. Pleines, M. Bernder, M. Austinat, M. Bösi, G. Stoll, B. Nieswandt, Orai1 (CRACM1) is the platelet SOC channel and essential for pathological thrombus formation, Blood 113 (2009) 2056–2063.

[23] K. Gilio, R. van Kruchten, A. Braun, A. Berna-Erro, M.A. Feijge, D. Stegner, P.E. van der Meijden, M.J. Kuijpers, D. Varga-Szabo, J.W. Heemskerk, B. Nieswandt, Roles of platelet STIM1 and Orai1 in glycoprotein VI- and thrombin-dependent procoagulant activity and thrombus formation, J. Biol. Chem. 285 (2010) 23629–29638.

[24] M. Nagy, T.G. Mastenbroek, N.J. Mattheij, S. de Witt, K.J. Clemetson, J. Kirschner, A. Schulz, A. Braun, J.M. Cosemans, B. Zieger, J.W. Heemskerk, Variable impairment of platelet functions in patients with severe, genetically linked immune deficiencies, Haematologica 103 (2018) 540–549.

[25] M.T. Harper, A.W. Poole, Store-operated calcium entry and non-capacitative calcium entry have distinct roles in thrombin-induced calcium signaling in human platelets, Cell Calcium 50 (2011) 351–358.

[26] M.P. Mahaut-Smith, S.J. Ennion, M.G. Rolf, R.J. Evans, ADP is not an agonist at P2X$_1$ receptors: evidence for separate receptors stimulated by ATP and ADP on human platelets, Br. J. Pharmacol. 131 (2000) 108–114.

[27] M.P. Mahaut-Smith, K.A. Taylor, R.J. Evans, Calcium signalling through ligand-gated ion channels such as P2X$_1$ receptors in the platelet and other non-excitable cells, Adv. Exp. Med. Biol. 898 (2016) 305–329.

[28] M.T. Harper, J.E. Camacho-Londono, K. Quick, J. Camacho-Londono, V. Flockerzi, S.E. Phillipp, L. Birnbaumer, M. Freichel, A.W. Poole, Transient receptor potential channels function as a coincidence signal mediating phosphatidylserine exposure, Sci. Signal. 6 (2013) ra50.

[29] G. Ramanathan, S. Gupta, I. Thielmann, I. Pleines, D. Varga-Szabo, F. May, C. Mannhalter, A. Dietrich, B. Nieswandt, A. Braun, Defective diacylglycerol-induced Ca^{2+} entry but normal agonist-induced activation responses in TRPC6-deficient mouse platelets, J. Thromb. Haemost. 10 (2012) 419–429.

[30] W. Chen, I. Thielmann, S. Gupta, H. Subramanian, D. Stegner, R. van Kruchten, A. Dietrich, S. Gambaryan, J.W. Heemskerk, H.M. Hermanns, B. Nieswandt, A. Braun, Orai1-induced store-operated Ca^{2+} entry enhances phospholipase activity and modulates canonical transient receptor potential channel 6 function in murine platelets, J. Thromb. Haemost. 12 (2014) 528–539.

[31] C. Bae, F. Sachs, P.A. Gottlieb, The mechanosensitive ion channel Piezo1 is inhibited by the peptide GsMTx4, Biochemistry 50 (2011) 6295–6300.

[32] A. Aliotta, D. Bertaggia Calderara, M.G. Zermatten, L. Alberio, Sodium-calcium exchanger reverse mode sustains dichotomous ion fluxes required for procoagulant COAT platelet formation, Thromb. Haemost. 121 (2021) 309–321.

[33] D.I. Fernandez, I. Provenzale, J. van Groningen, B.M.E. Tullemans, A. Veninga, J. L. Dunster, S. Honarnejad, H. van den Hurk, M.J. Kuijpers, J.W. Heemskerk, Ultra-high throughput Ca^{2+} response patterns in platelets to distinguish between ITAM-linked and G- protein coupled receptor activation, iScience. 25 (2022), 103718.

[34] K. Gilio, I.C. Munnix, P. Mangin, J.M. Cosemans, M.A. Feijge, P.E. van der Meijden, S. Olieslagers, M.B. Chrzanowska-Wodnicka, R. Lillian, S. Schoenwaelder, S. Koyasu, S.O. Sage, S.P. Jackson, J.W. Heemskerk, Non-redundant roles of phosphoinositide 3-kinase isoforms alpha and beta in glycoprotein VI-induced platelet signaling and thrombus formation, J. Biol. Chem. 284 (2009) 33750–33762.

[35] M.A. Feijge, E.C. van Pampus, C. Lacabaratz-Porret, K. Hamulyak, S. Lévy-Toledano, J. Enouf, J.W. Heemskerk, Inter-individual varability in Ca^{2+} signalling in platelets from healthy volunteers, relation with expression of endomembrane Ca^{2+}-ATPases, Br. J. Haematol. 102 (1998) 850–859.

[36] P. Sargeant, W.D. Clarkson, S.O. Sage, J.W. Heemskerk, Calcium influx in Fura-2-loaded human platelets is evoked by thapsigargin and 2,5-di-(t-butyl)-1,4-benzo-hydroquinone and reduced by inhibitors of cytochrome P-450, Cell Calcium 13 (1992) 553–564.

[37] J.W. Heemskerk, M.A. Feijge, S.O. Sage, U. Walter, Indirect regulation of Ca^{2+} entry by cAMP-dependent and cGMP-dependent protein kinases and phospholipase C in rat platelets, Eur. J. Biochem. 223 (1994) 543–551.

[38] I.M. Keularts, R.M. van Gorp, M.A. Feijge, M.W. Vuist, J.W. Heemskerk, a$_{2A}$-Adrenergic receptor stimulation potentiates calcium release in platelets by modulating cAMP levels, J. Biol. Chem. 275 (2000) 1763–1772.

[39] A. Veninga, C.C. Baaten, B.M. Tullemans, I. De Simone, M.J. Kuijpers, J. W. Heemskerk, P.E. van der Meijden, Effects of platelet agonists and priming on the formation of platelet populations, Thromb. Haemost. 122 (2022) 726–738.

[40] N.J. Jooss, I. De Simone, I. Provenzale, D.I. Fernandez, S.L. Brouns, R.W. Farndale, Y.M. Henskens, M.J. Kuijpers, H. ten Cate, P.E. van der Meijden, R. Cavill, J. W. Heemskerk, Role of platelet glycoprotein VI and tyrosine kinase Syk in thrombus formation on collagen-like surfaces, Int. J. Mol. Sci. 20 (2019) e2788.

[41] G. Grynkiewicz, M. Poenie, R.Y. Tsien, A new generation of Ca^{2+} indicators with greatly improved fluorescence properties, J. Biol. Chem. 260 (1985) 3440–3450.

[42] J.P. Van Geffen, S.L. Brouns, J. Batista, H. McKinney, C. Kempster, M. Nagy, S. Sivaparatnam, C.C. Baaten, N. Bourry, M. Frontini, K. Jurk, M. Krause, D. Pillitteri, F. Swieringa, R. Verdoold, R. Cavill, M.J. Kuijpers, W.H. Ouwehand, K. Downes, J.W. Heemskerk, High-throughput elucidation of thrombus formation reveals sources of platelet function variability, Haematologica 104 (2019) 1256–1267.

[43] J.G. White, Platelet structure, in: A Michelson (Ed.), Platelet structure, Platelets (2007) 45–73, pages.

[44] J.W. Heemskerk, G.M. Willems, M.B. Rook, S.O. Sage, Ragged spiking of free calcium in ADP-stimulated human platelets: regulation of puff-like calcium signals in vitro and ex vivo, J. Physiol. 535 (2001) 625–635.

[45] P. Sargeant, S.O. Sage, Calcium signalling in platelets and other nonexcitable cells, Pharmacol. Ther. 64 (1994) 395–443.

[46] A. Malayev, D.J. Nelson, Extracellular pH modulates the Ca^{2+} current activated by depletion of intracellular Ca^{2+} stores in human macrophages, J. Membr. Biol. 146 (1995) 101–111.

[47] A. Beck, A. Fleig, R. Penner, C. Peinelt, Regulation of endogenous and heterologous Ca^{2+} release-activated Ca^{2+} currents by pH, Cell Calcium 56 (2014) 235–243.

[48] M.D. Bootman, T.J. Collins, L. Mackenzie, H.L. Roderick, M.J. Berridge, C. M. Peppiatt, 2-aminoethoxydiphenyl borate (2-APB) is a reliable blocker of store-operated Ca^{2+} entry but an inconsistent inhibitor of InsP$_3$-induced Ca^{2+} release, FASEB J. 16 (2002) 1145–1150.

[49] R. Van Kruchten, A. Braun, M.A. Feijge, M.J. Kuijpers, R. Rivera-Galdos, P. Kraft, G. Stoll, G. Kleinschnitz, E.M. Bevers, B. Nieswandt, J.W. Heemskerk, Antithrombotic potential of blockers of store-operated calcium channels in platelets, Arterioscler. Thromb. Vasc. Biol. 32 (2012) 1717–1723.

[50] A. Kondratskyi, M. Yassine, C. Slomianny, K. Kondratska, D. Gordienko, E. Dewailly, V. Lehen'kyi, R. Skryma, N. Prevarskaya, Identification of ML-9 as a lysosomotropic agent targeting autophagy and cell death, Cell Death Dis. 5 (2014) e1193.

[51] L. Waldherr, A. Tiffner, D. Mishra, M. Sallinger, R. Schober, I. Frischauf, T. Schmidt, V. Handl, P. Sagmeister, M. Köckinger, I. Derler, M. Üçal, D. Bonhenry, S. Patz, R. Schindl, Blockage of store-operated Ca^{2+} influx by Synta66 is mediated by direct inhibition of the Ca^{2+} selective Orai1 pore, Cancers (Basel) 12 (2020) 2876.

[52] B.L. Lin, D. Matera, J.F. Doerner, N. Zheng, D. Del Camino, S. Mishra, H. Bian, et al., In vivo selective inhibition of TRPC6 by antagonist BI 749327 ameliorates fibrosis and dysfunction in cardiac and renal disease, Proc. Natl. Acad. Sci. USA. 116 (2019) 10156–10161.

[53] Y. Tan, W. Lu, X. Yi, H. Cai, Y. Yuan, S. Zhang, Improvement of platelet preservation by inhibition of TRPC6, Transfus Med (2023) in press.

[54] Z. Ilkan, J.R. Wright, A.H. Goodall, J.M. Gibbins, C.I. Jones, M.P. Mahaut-Smith, Evidence for shear-mediated Ca^{2+} entry through mechanosensitive cation channels in human platelets and a megakaryocytic cell line, J. Biol. Chem. 292 (2017) 9204–9217.

[55] M.T. Harper, M.J. Mason, S.O. Sage, A.G. Harper, Phorbol ester-evoked Ca^{2+} signaling in human platelets is via autocrine activation of P2X$_1$ receptors, not a novel non-capacitative Ca^{2+} entry, J. Thromb. Haemost. 8 (2010) 1604–1613.

[56] F.M. Bennett, J.I. Mobbs, S. Ventura, D.M. Thal, The P2X$_1$ receptor as a therapeutic target, Purinergic Sign 18 (2022) 421–433.

[57] N. Jost, N. Nagy, C. Corici, Z. Kohajda, A. Horváth, K. Acsai, P. Biliczki, J. Levijoki, P. Pollesello, T. Koskelainen, L. Otsomaa, A. Tóth, J.G. Papp, A. Varró, L. Virág, ORM-10103, a novel specific inhibitor of the Na$^+$/Ca^{2+} exchanger, decreases early and delayed afterdepolarizations in the canine heart, Br. J. Pharmacol. 170 (2013) 768–778.

[58] A. Kholmukhamedov, R. Janecke, H.J. Choo, S.M. Jobe, The mitochondrial calcium uniporter regulates procoagulant platelet formation, J. Thromb. Haemost. 16 (2018) 2315–2321.

[59] M.H. Flamm, T.V. Colace, M.S. Chatterjee, H. Jing, S. Zhou, D. Jaeger, L.F. Brass, T. Sinno, S.L. Diamond, Multiscale prediction of patient-specific platelet function under flow, Blood 120 (2012) 190–198.

[60] L. Joutsi-Korhonen, P.A. Smethurst, A. Rankin, E. Gray, M. IJsseldijk, C.M. Onley, N.A. Watkins, L.M. Williamson, A.H. Goodall, P.G. de Groot, R.W. Farndale, W. H. Ouwehand, The low-frequency allele of the platelet collagen signaling receptor glycoprotein VI is associated with reduced functional responses and expression, Blood 101 (2003) 4372–4379.

[61] C.C. Baaten, H. ten Cate, P.E. van der Meijden, J.W. Heemskerk, Platelet populations and priming in hematological diseases, Blood Rev. 31 (2017) 389–399.

[62] M.S. Chatterjee, J.E. Purvis, L.F. Brass, S.L. Diamond, Pairwise agonist scanning predicts cellular signaling responses to combinatorial stimuli, Nat. Biotechnol. 28 (2010) 727–732.

[63] A.T. Dolan, S.L. Diamond, Systems modeling of Ca^{2+} homeostasis and mobilization in platelets mediated by IP$_3$ and store-operated Ca^{2+} entry, Biophys. J. 106 (2014) 2049–2060.

[64] J.I. Goto, A.Z. Suzuki, S. Ozaki, N. Matsumoto, T. Nakamura, E. Ebisui, A. Fleig, R. Penner, K. Mikoshiba, Two novel 2-aminoethyl diphenylborinate (2-APB) analogues differentially activate and inhibit store-operated Ca^{2+} entry via STIM proteins, Cell Calcium 47 (2010) 1–10.

[65] J. Huang, F. Swieringa, F.A. Solari, I. Provenzale, L. Grassi, I. De Simone, C. C. Baaten, R. Cavill, A. Sickmann, M. Frontini, J.W. Heemskerk, Assessment of a complete and classified platelet proteome from genome-wide transcripts of human platelets and megakaryocytes covering platelet functions, Sci. Rep. 11 (2021) 12358.

[66] B.B. Dawood, J. Wilde, S.P. Watson, Reference curves for aggregation and ATP secretion to aid diagnose of platelet-based bleeding disorders: effect of inhibition of ADP and thromboxane A$_2$ pathways, Platelets 18 (2007) 329–345.

[67] OMIM, OMIM online catalog of human genes and genetic disorders, http://omim.org. (2023).

[68] J.M. Burkhart, M. Vaudel, S. Gambaryan, S. Radau, U. Walter, L. Martens, J. G, A. Sickmann, R.P. Zahedi, The first comprehensive and quantitative analysis of human platelet protein composition allows the comparative analysis of structural and functional pathways, Blood 120 (2012) e73–e82.

[69] M. Zeiler, M. Moser, M. Mann, Copy number analysis of the murine platelet proteome spanning the complete abundance range, Mol. Cell. Proteomics. 13 (2014) 3435–3445.